SYSTEMATIC DESIGN OF COMPLIANT MORPHING STRUCTURES WITH STIMULUS AS DESIGN AND STATE VARIABLE

SYSTEMATIC DESIGN OF COMPLIANT MORPHING STRUCTURES WITH STIMULUS AS DESIGN AND STATE VARIABLE

By JAMAL SHABANI, B.Sc., M.Sc.

A Thesis Submitted to the School of Graduate Studies in Partial Fulfillment of the Requirements for the Degree Doctor of Philosophy

Doctor of Philosophy (2024) McMaster University
Department of Mathematics and Statistics Hamilton, Ontario, Canada

TITLE:	Systematic design of compliant morphing structures with stimulus as design and state variable
AUTHOR:	Jamal Shabani B.Sc. (Middle East Technical University), M.Sc. (Louisiana State University).
SUPERVISOR:	Dr. Blaise Bourdin
NUMBER OF PAGES:	xvii, 107

Abstract

Advances in additive manufacturing and synthesis of complex "responsive" materials whose properties can be altered through external stimuli are opening the door to a new generation of integrated devices and materials. While manufacturing such structures or materials has received a considerable attention (see for instance [71, 85]), their actual design remains challenging. Starting from the pioneering works of [73, 56, 52], topology optimization has established itself as a powerful tool for systematic design of micro-devices, Micro Electro Mechanical Systems (MEMS), or materials microstructures. Topology optimization aims to answer the question, what is the optimal distribution of materials in a ground domain in order to optimize a given objective function subject to some constraints? Mathematically, topology optimization is formulated as a PDE-constrained optimization, conventionally employing Finite Elements Methods (FEM) to solve the underlying PDE constraints. In this thesis, we study optimal design of responsive structures made of several materials, with at least one of the materials is responsive material, though topology optimization. The objective of the present work is to algorithmically find the distribution of materials in a ground domain that optimizes an objective function [25]. It is well-known that such problems are generally ill-posed (see [5] for instance) resulting in optimal designs consisting of an infinitely fine mixture of multiple materials. Homogenization approaches [35, 8, 5, 7]

tackle this problem directly by extending admissible designs to such mixtures. This type of approach is mathematically well grounded and leads to well posed problems that can be implemented efficiently. However, it is often criticized for leading to designs that cannot be manufactured. Several other classes of techniques aim at restricting the class of admissible designs in such a way that avoids fine mixtures. The combination of material interpolation (SIMP) and filters [21, 27] is a commonly employed approach. Shape parameterization by level set functions [10, 12] also limits the complexity of designs. Finally, by penalizing the length (or surface) of interfaces between materials, perimeter penalization [16, 50, 66] also produces designs with limited complexity. Additionally, perimeter penalization can be efficiently implemented using a phase-field approach [28, 29, 82].

In this work, we propose a phase-field algorithm for the systematic design of responsive structures achieving prescribed deformations under some unknown distributions of a stimulus. Our focus is on linear elastic materials in which an external stimulus can generate an isotropic inelastic strain, similar to linear thermo-elastic materials. We begin by providing mathematical analysis of the problem and review classical optimal design methods and finally we detail the phase-field approach to optimal design. We introduce the responsive minimimum compliance problem of linear elastic structures. After giving the intricacies of this seemingly simple problem, we introduce the phase-field model to prove the existence of a solution and provide a numerical implementation. We then turn to the design of compliant morphing linear elastic structures. Here we begin by considering design of responsive structure that can move in a prescribed direction upon activation by a stimulus. We demonstrate the stregth of our approach by studying the optimal design of 2D structures consisting

of void, one non-responsive material and one responsive material. Next, we explore the design of time-dependent compliant morphing linear elastic structures. Here we consider the stimulus to be a state variable controlled by the transient heat equations.

We conclude by summarizing the presented work and discuss the its contribution towards the overarching goal of optimal design for responsive structure.

Acknowledgements

There are so many people that had an enormous help in my graduate studies through their guidance, motivation, and support. Here, I would like to mention few of these people and their contributions. This includes advisors, thesis committee members, past and present group members, collaborators, friends, and most importantly family.

First, I would like to express my sincere gratitude towards to my advisor Dr. Blaise Bourdin for his patience and unwavering support through my graduate studies from Louisiana State University to now at McMaster University. I am very thankful for time he sacrificed for our weekly meetings, his enlightening discussions and ideas motivated me to study harder. I would like to thank Dr. Bartosz Protas and Dr. Lia Bronsard for serving on my PhD supervisory committee.

Second, I would like to thank the past and current group members. I have learned quite a lot from our discussions. In particular, it has been a pleasure having discussion with Dr. Nha Van Tran his short lecture on adjoint methods helped me alot to understand and to use adjoint methods in my computations. Also I would like to thank current group members Samba Dumbaya and Dr. Pooya Yousefi, a postdoc in our current group. Our friday weekly meeting provided lots of useful insights into $\Gamma-$ convergence. I have also had the opportunity to work with incredible collaborators. I have learned alot working with Kaushik Bhattacharya and this former student Dr.

Andrew Akerson on optimal design of responsive structures. I also would like to thank Professor Xin Yang Lu for agreeing to serve as an external examiner.

Third, I must thank my wonderful family especially my mother, for her immense patience, encouragement and support through all my ups and downs. Her love and support has allowed me to pursue my research towards the successful thesis you see before.

Finally, Support for this work was provided in part by the National Science Foundation (NSF), Applied Mathematics Program: "Collaborative Research: Optimal Design of Responsive Materials and Structures", under grants DMS-2009303. Any opinions, findings, and conclusions or recommendations expressed in this material are those of the author and do not necessarily reflect the views of the National Science Foundation.

Contents

List of Figures

List of Tables

List of Abbreviations

2D	Two Dimensional
3D	Three Dimensional
BNCG	Bounded Nonlinear Conjugate Gradient
BV	Functions of Bounded Variations
FEM	Finite Element Method
MEMS	Micro Electro Mechanical Systems
PDE	Partial Differential Equation
PETSc	Portable, Extensible Toolkit for Scientific Computation
SIMP	Solid Isotropic Material with Penalisation
TAO	Toolkit for Advanced Optimization
UFL	Unified Form Language

Chapter 1

Introduction

In the last two decades, the advances in modern manufacturing processes, such as additive manufacturing and synthesis of complex "responsive" materials whose properties can be altered through external stimuli, have resulted in a high interest in optimal design as a means of designing high performance structures with high degrees of geometrical complexity. These structures are built by integrating responsive materials such as shape-memory alloys, piezoelectrics, dielectric elastomers and liquid crystal elastomers with non-responsive materials. However the design of such integrated structures remains challenging, it is important to develop a systematic design methodology. This thesis explores this through optimal design methods.

1.1 Optimal design

The main objective of optimal design problem is to solve the inverse problem of finding the distribution of several materials and void or holes that optimizes the performance of a structure. The subject of optimal design was originally introduced in late 19th

century by James Clark Maxwell [60] and much of the recent developments have occurred in the past few decades [59] where the subject has been extensively formulated for optimizing simple objective functions using basic mechanics models. Today, there is a rich literature on the subject of optimal design and this thesis will base on the pioneering work of [73, 56, 52]. The important terminologies used in optimal design problems are outlined as follows:

An objective function measures the performance of the structure. The performance of the structure is improved through optimizing (maximizing or minimizing) a given objective function [9, 25]. The objective function that one seeks to optimize to achieve an optimal solution, may involve state variables and can be directly or indirectly dependent on the design variables and subject. Examples of objective functions include *maximizing stiffness, minimizing cost and minimizing weight or volume.*

Design variables consist of a group of parameters that define the structure. The design variables can either be discrete or continuous. There are design constraints that are usually imposed on design variables. These constraints can typically be imposed in two ways: equality and inequality constraints. The equality constraint is when the design variables must meet a specific criteria, such as equilibrium equations in a structural problem. The inequality constraint is when the design variables must remain in a specific criteria region, such as lower and upper bounds. Examples of design variables include *length, thickness and material density.*

A state variable defines the mechanical behavior of the structure. The state variable is usually computed by solving an underlying Partial Differential Equation (PDE) constraint. Examples of state variables include *displacement field and temperature field.* In these cases the underlying PDE constraints could be *the equations of linearized*

elasticity PDE (resp. transient heat PDE) for displacement field (resp. temperature field).

1.1.1 Optimal design categories

Optimal design problems can roughly be classified into the following three categories from [6, 45]:

Sizing optimization

In sizing optimization, designs structure is parametrized by a few design variables implying that the set of admissible designs is considerably simplified. Size optimization involves finding the optimal dimensions in a design structure while its shape is fixed throughout the optimization process. Examples of sizing optimization includes *finding the optimal cross sectional area, thickness, length and width of the design* [22].

Shape optimization

In shape optimization, the optimal designs are obtained from an initial guess by moving its boundary without changing its topology, *i.e.*, its number of holes in 2D. Here, the structure is assumed to have a set number of holes, with the shape of them considered as the optimized quantity. In this approach the design variables are often a set of points on the geometry being optimized, and their cartesian coordinates are iteratively updated until an optimum is reached [11].

Topology optimization

In topology optimization, both the shape and the topology of the admissible designs can vary without any explicit or implicit restrictions. Topology optimization extends size and shape optimization further and gives no restrictions to the structure that is to be optimized. Topology optimization is the most computational expensive and powerful of the three categories as it does not involve any predefined configurations [25, 76]. For this reason, topology optimization is very useful tool in many areas of design and goal of topology optimization is to create an optimal design that is strong and lightweight, and that can withstand the applied loads without failing. The concept was initiated for mechanical design problems but has spread to a wide range of other physical disciplines, including fluids, electromagnetics, optics and combinations thereof [76].

Topology optimization can be solved through density-based methods where the density of material at each point in the domain is unknown and the design problem is posed as an optimization problem over these unknown densities. Then, gradient-based optimization methods are used to iteratively update the design, where sensitivities are usually computed through the adjoint method [67].

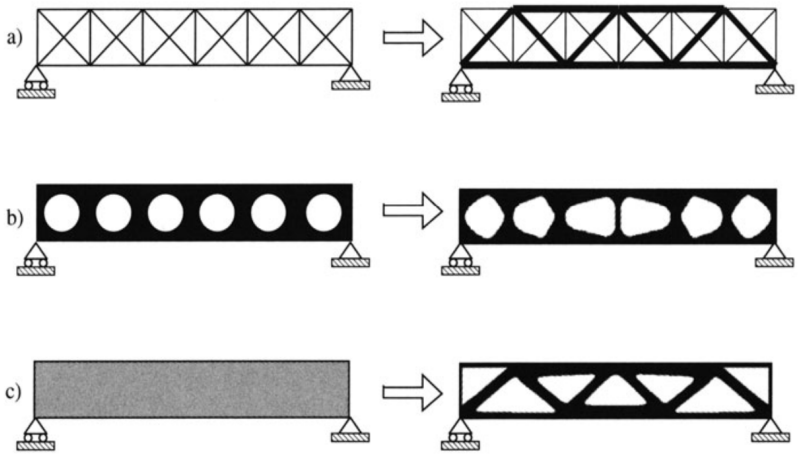

Figure 1.1: The ground domain (left) and converged design (right) for sizing optimization (a), shape optimization (b), and topology optimization (c). *Source [25]*

Definition 1.1.1. *The ground domain, Ω is a 2-dimensional area or 3-dimensional volume in which the optimal design can be contained.*

The typical topology optimization problem is concerned of finding the partition of the ground domain

$$\Omega = (D_1, D_2, \ldots, D_m) \text{ such that } \bigcup_{i=1}^{m} \overline{D_i} = \overline{\Omega} \tag{1.1.1}$$

where each D_i is occupied by material i, maximizing or minimizing some general objective function $\mathcal{I}(u_1, u_2, \ldots, u_n)$ depending on state variable u_j satisfying a state PDE. Unconstrained topology optimization problems often lead to trivial solutions (for example, in a case of classical minimum compliance, a trivial solution would be a

structure consists 100% of the stiffest material), so we consider a topology optimization problems with constraints on both the state and design variables. Constraints on design variables include prescribing the material occupying specific regions of the domain, bounds on the volume fraction of each material and box constraints (lower and upper bounds). Constraints on the state variables include prescribing maximum displacement on some part of the boundary and maximum bounds on the maximum point-wise stress in the minimum compliance problem [9, 24, 57].

Mathematically, a general constrained topology optimization problem is of the form:

$$\begin{aligned} &\text{minimize} && \mathcal{I}(u_1, u_2, \ldots, u_n) \\ &\text{subject to} && \mathrm{C}_i(\Phi, u_i) = 0,\ i = 1, 2, \ldots, n \\ & && \mathrm{H}_j(\Phi) \leq 0,\ j = 1, 2, \ldots, k \end{aligned} \tag{1.1.2}$$

where $\mathcal{I}$ denotes the objective function. Here, C_i and H_j represent equality and inequality constraints, that can be interpreted as restrictions on the state variables u_i and the design variable Φ. The typical equality constraints in constrained topology optimization problems are the state PDEs modelling u_i, *i.e* controlling the mechanical behaviour of the structure and the inequality constraints are the bound on allowed volume of materials inside Ω and box constraints on design variable Φ.

A classical example of topology optimization is the minimum compliance problem where the objective function represents

$$\mathcal{I}(u) = \int_{\partial\Omega} f \cdot u \, ds \tag{1.1.3}$$

the compliance measuring the work done by an applied load f. Hence minimizing this quantity minimizes the deflection of the structure due to an applied load and

thus maximizes the overall stiffness of the structure.

Figure (1.2) below shows an example of the classical minimum compliance in 2D where the ground domain Ω is fixed at the left end. The white region in the design represents void and grey region is the optimal allocation of the material to maximize the stiffness of the design.

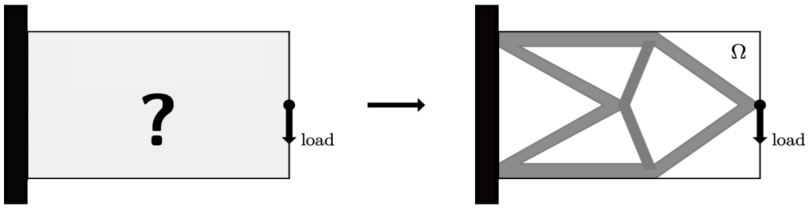

Figure 1.2: Illustration of classical minimum compliance problem.

The main focus of the present work will be restricted to optimal design of responsive structures using topology optimization. In optimal design of responsive structure, one or more of the materials used in design is an active or responsive material. Responsive materials are those materials whose properties such as shape and/or stiffness can be changed by external stimulus. External stimulus includes electrical or magnetic fields, temperature, light and heat. It is now becoming possible to 3D print responsive materials like shape-memory alloys (SMA), shape of SMA can be affected by change in temperature and liquid crystal elastomers (LCEs), shape of LCEs can be affected by change in heat. This paves the way for responsive structures whose shape can be controlled by external stimulus. Further, combining them with other non-responsive materials can endow them with functions that are of use for many

applications including soft robotics, wearable and prosthetic devices. Figure (1.3) below shows a responsive wrist like structure designed using SMA and its action upon actuation.

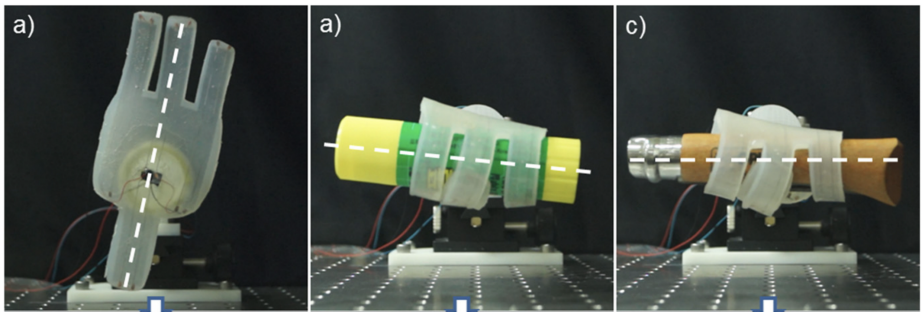

Figure 1.3: Wrist actuation using SMA. *Source [69].*

However, actual design of such responsive structures remains challenging, this project will develop a methodology for the systematic design of responsive structures and meta-materials which are assemblies of distinct materials and voids, especially optimal design where one seeks the best function at the least cost. We seek the optimal distribution of the responsive material, non-responsive materials and void and optimal stimulus that minimize some objective function.

1.2 Outline of the Thesis

In this thesis, we propose a phase-field algorithm for the systematic design of responsive structures achieving prescribed deformations under some unknown distributions of a stimulus. Our focus is on linear elastic materials in which an external stimulus can generate an isotropic inelastic strain, similar to linear thermo-elastic materials. The thesis is structured as follows:

- In **Chapter 2**, the theoretical background necessary for the understanding and

reproduction of the thesis is provided. We set the Hilbert and Sobolev spaces on the ground domain Ω [1, 49]. We introduce the responsive optimal design problem and discuss the classical attempts to solve the problem and present the phase-field approach to optimal design and discuss the well-known adjoint method for sensitity.

The content of **Chapter 2** is based on [68, 30, 32–34, 36, 38, 46, 53]

- In **Chapter 3**, we introduce the responsive minimum compliance problem for an isotropic linear elastic structure. As the naive formulation results in an ill-posed optimization problem, we discuss regularization through the phase-field approach to optimal design. Finally, we detail the numerical implementation and give some numerical results.

- In **Chapter 4**, we focus on systematic design of compliant morphing structures where the stimulus is a design variable. We provide the proof of existence of solutions to the responsive optimal design through the classical $\Gamma-$convergence for phase transition problem [62, 61, 77, 3]. We present two numerical implementation schemes and finally we explore integrated structures composed of void, responsive and non-responsive materials for use in actuation.

  The content of **Chapter 4** is verbatim from a submitted paper [72] and therefore contains some reduntant material.

- In **Chapter 5**, we extend **Chapter 4** by considering the stimulus as a state variable. This leads to systematic design of time-dependent compliant morphing structures where the stimulus changes with respect to both time and space. Here, the stimulus is controlled through the equations of transient heat PDEs.

Chapter 2

Notation and Preliminaries

2.1 L^p Spaces and Sobolev Spaces

Let us start introducing some important notations and preliminaries. Throughout this thesis Ω is an open bounded subset of $\mathbb{R}^d$, where $d = 2, 3$.

Definition 2.1.1. *If $u : \Omega \to \mathbb{R}$ is a measurable function and $1 \leq p < \infty$, we define*

$$\|u\|_p = \left(\int_\Omega |u|^p \, dx \right)^{\frac{1}{p}}.$$

If $p = \infty$, we define

$$\|u\|_\infty = \inf\{M \geq 0 : |u| \leq M \ a.e\}.$$

The space $L^p(\Omega)$ is defined as

$$L^p(\Omega) = \{u : \Omega \to \mathbb{R} : \|u\|_p < \infty, u \text{ is measurable}\},$$

for $1 \leq p < \infty$. *For a sequence* (u_n), *we say* $u_n \to u$ *in* $L^p(\Omega)$, *if*

$$\|u_n - u\|_p \to 0.$$

The functions in the space for solutions of differential equations might not have a smooth derivative or are not even differentiable. The space we use to find solution for differential equations is the Sobolev space.

For now suppose $u \in C^k(\Omega)$, where $k \in \mathbb{N}$, and $\phi \in C_0^\infty(\Omega)$. The spaces $C^k(\Omega)$ consists of function with k continuous derivatives and $C_0^\infty(\Omega)$ consists of smooth functions that have compact support and continuous derivatives of all orders. Let $\alpha = (\alpha_1, \alpha_2, \ldots, \alpha_n) \in \mathbb{N}^n$ be a multi-index such that $|\alpha| = \alpha_1 + \alpha_2 + \cdots + \alpha_n \leq k$. Repeated integration by parts gives

$$\int_\Omega u D^\alpha \phi \, dx = (-1)^{|\alpha|} \int_\Omega \phi D^\alpha u \, dx \tag{2.1.1}$$

where

$$D^\alpha u = \frac{\partial^{|\alpha|} u}{\partial_{x_1}^{\alpha_1} \cdots \partial_{x_n}^{\alpha_n}}.$$

Note that the boundary terms are equal to zero because $\phi = 0$ on the boundary of Ω. If $u \notin C^k(\Omega)$, the derivative of u in (2.1.1) does not make sense in the classical way. We need to define what the derivative means for functions that are not continuously differentiable.

Definition 2.1.2. *Suppose* $u \in L^1(\Omega)$ *and* α *is a multi-index. If* $v \in L^1(\Omega)$ *satisfies,*

$$\int_\Omega u D^\alpha \phi \, dx = (-1)^{|\alpha|} \int_\Omega \phi v \, dx,$$

then v is the αth weak partial derivative of u. We denote the weak derivative by

$$D^\alpha u = v.$$

Note that if $u \in C^k(\Omega)$, then the weak derivative coincides with the classical definition of derivative.

Definition 2.1.3. *The Sobolev space $W^{k,p}(\Omega)$ consists of functions in $L^p(\Omega)$ such that the weak derivatives up to order k are in $L^p(\Omega)$ as well*

$$W^{k,p}(\Omega) = \{u \in L^p(\Omega) : D^\alpha u \in L^p(\Omega) \ \ \forall |\alpha| \leq k\}.$$

The associated norm for $1 \leq p < \infty$ is defined by

$$\|u\|_{k,p} = \left(\sum_{|\alpha| \leq k} \int_\Omega |D^\alpha u|^p \, dx \right)^{\frac{1}{p}}.$$

If $p = \infty$, the norm is defined by

$$\|u\|_{k,\infty} = \sum_{|\alpha| \leq k} \|D^\alpha u\|_\infty.$$

If $p = 2$, the Sobolev spaces $W^{k,2}(\Omega)$ are Hilbert spaces, and we denote them by $H^k(\Omega)$. The inner product of $H^k(\Omega)$ is defined by

$$\langle u, v \rangle_{H^k} = \sum_{i=0}^{k} \langle D^i u, D^i v \rangle_{L^2}.$$

2.2 Lower semicontinuity and Coercivity

The concepts of lower semicontinuity and coercity are very important in minimization problems. Given a real valued functional F on a set X, one of the main problem of the calculus of variations is to find the minimum value

$$\min(F) = \inf_{y \in X} F(y)$$

and the corresponding minimum point x such that

$$F(x) = \inf_{y \in X} F(y).$$

Definition 2.2.1. *A sequence (y_n) is called minimizing sequence if*

$$\lim_{n \to \infty} F(y_n) = F(x) = \inf_{y \in X} F(y).$$

Definition 2.2.2. *A function $F : X \to \mathbb{R}$ is said to be lower semicontinuous (l.s.c. for short) if for every sequence $x_n \to x$ in X we have*

$$F(x) \leq \liminf F(x_n).$$

Informally, a function is lower semicontinuous if it is continuous or, if not, it only jumps down as shown in Figure (2.1) [55].

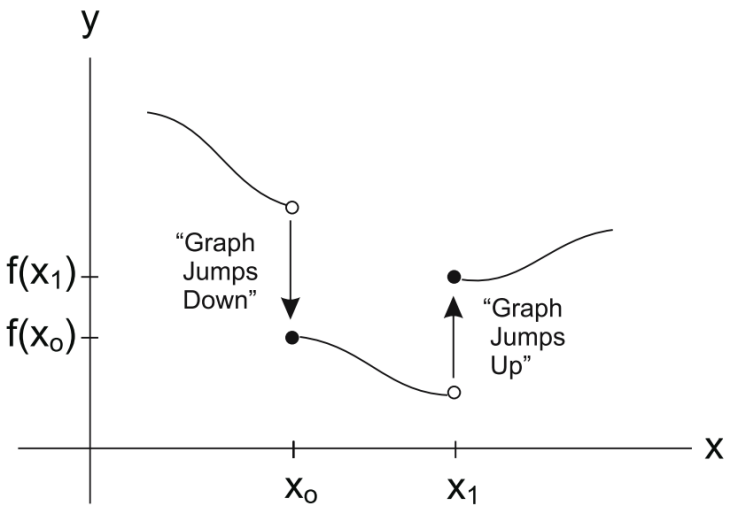

Figure 2.1: A function that is lower semicontinuous at x_0 but not lower semicontinuous at x_1.

In this figure above, we see that

$$\liminf_{x\to x_0} f(x) = f(x_0) \text{ and } \limsup_{x\to x_1} f(x) = f(x_1)$$

and therefore f is lower semicontinuous at x_0 and not at x_1 as it "jumps down" at x_0 and "jumps up" at x_1.

Definition 2.2.3. *A function $F : X \to \mathbb{R}$ is said to be coercive, if for every $t \in \mathbb{R}$ the set*

$$\{x \in X : F(x) \leq t\}$$

is precompact.

Equivalently, coercivity can be defined in terms of convergence of subsequences.

Definition 2.2.4. *A function $F : X \to \mathbb{R}$ is coercive if every sequence (x_n) such that $\limsup F(x_n) < \infty$ has a convergent subsequence.*

Theorem 2.2.1. *If function $F : X \to \mathbb{R}$ is lower semicontinuous and coercive. Then F has a minimum point in X.*

Proof. Suppose now that F is not identically $+\infty$. Let (y_n) be a minimizing sequence for F in X. Since F is coercive $y_n \to x \in X$ up to subsequence. We have

$$\lim F(y_n) = \inf_{y \in X} F(y) \leq F(x) \leq \liminf F(y_n)$$

which proves x minimum point of F. □

Definition 2.2.5. *We say that the sequence $F_n : X \to \mathbb{R}$ is equi-coercive if for every $t \in \mathbb{R}$ there exists a closed countably compact subset K_t of X such that*

$$\{x \in X : F_n \leq t\} \subseteq K_t \; \forall n \in \mathbb{N}.$$

Proposition 2.2.2. *The sequence (F_n) is equi-coercive if there exists a lower semi-continuous coercive function $\Psi : X \to \mathbb{R}$ such that $F_n \geq \Psi$ for every $n \in \mathbb{N}$.*

Proof. If such a function Ψ exists, then (F_n) is equi-coercive, since

$$\{F_n \leq t\} \subseteq \{\Psi \leq t\}$$

for every $n \in \mathbb{N}$ and for every $t \in \mathbb{R}$, and the sets $K_t = \{\Psi \leq t\}$ are closed and countably compact. □

2.3 $\Gamma-$Convergence

We introduce the notion of $\Gamma-$convergence which is very useful in minimization problems. The notion of $\Gamma-$convergence was introduced by Ennio De Giorgi in a sequence of papers (cf. [40–42]). An excellent account of this concept is the book of Dal Maso [39] and Andrea Braides [32].

Definition 2.3.1. *Let $F : X \to \mathbb{R}$ and $F_n : X \to \mathbb{R}$, where X is a topological space. We say, F_n $\Gamma-$converges to F if the following two conditions hold for any $x \in X$.*

1. *(liminf inequality): for every sequence $(x_n) \in X$ such that $x_n \to x$*

$$F(x) \leq \liminf_{n\to\infty} F_n(x_n).$$

2. *(limsup inequality): there exists a recovering sequence $(x_n) \in X$ with $x_n \to x$ such that*

$$F(x) \geq \limsup_{n\to\infty} F_n(x_n).$$

Suppose we are interested in finding the minimizer of a functional F. We can approximate F by a sequence of functionals F_n such that F_n $\Gamma-$converges to F. Using the Fundamental Theorem of $\Gamma-$convergence below, we see that the minimizers of F_n can be used to approximate the minimizer of F with additional assumption of *equi-coerciveness* on F_n *i.e*

$$\Gamma - \text{convergence} + \text{equi-coerciveness} \implies \text{convergence of minimizers.}$$

Theorem 2.3.1. *(Fundamental Theorem of $\Gamma-$Convergence) Let X be a topological*

space. Let (F_n) be an equi-coercive sequence of functions and let F_n $\Gamma-$converges to F in X, then the minimizers of F_n converge to a minimizer of F.

Proof. Let $y \in X$, and (y_n) be a recovery sequence for y i.e, $y_n \to y$. Then by (*limsup inequality*) condition above, we have

$$\limsup_{n\to\infty} F_n(y_n) \leq F(y). \tag{2.3.1}$$

Let x_n be minimizer of F_n, since F_n are equi-coercive, x_n belongs to some compact set of X and therefore we can find $x \in X$ such that $x_n \to x$ up to subsequence. We want to show that x is the minimizer of F. By using (*liminf inequality*) condition above, we have

$$F(x) \leq \liminf_{n\to\infty} F_n(x_n). \tag{2.3.2}$$

It follows that

$$F(x) \leq \liminf_{n\to\infty} F_n(x_n) \leq \limsup_{n\to\infty} F_n(x_n) \leq \limsup_{n\to\infty} F_n(y_n) \leq F(y) \ \ \forall y \in X.$$

We have shown that $F(x) \leq F(y)\ \forall y \in X$ and this means x is the minimizer of F. □

With the notion of $\Gamma-$convergence, we can now introduce the most important property of $\Gamma-$convergence.

Lemma 2.3.2. *($\Gamma-$convergence is stable under continuous perturbations): If $F_n \xrightarrow{\Gamma} F$ and G is continuous, then*

$$F_n + G \xrightarrow{\Gamma} F + G$$

Proof. It is clear that since G is continuous, then G satistifies both (*liminf inequality*) and (*limsup inequality*) conditions in $\Gamma-$convergence definition. Now if we take any

sequence $x_n \to x$, then the desired results follows directly from the properties of $\liminf$ and $\limsup$ for sum of two sequences. □

We recall examples of $\Gamma-$convergence in the framework of the calculus of variations, *i.e* we consider integral functionals defined on functional spaces where the integral functionals in question depend on a small parameter ε. One of the most classical example of $\Gamma-$convergence is given in the paper by Modica and Mortola [62, 63] where this result is also proven. This result is concerned with the approximation of the perimeter functional via some functionals which are more typical for the calculus of variations, *i.e* integral functionals involving the squared norm of the gradient. This $\Gamma-$convergence result is particularly interesting for numerical reasons; indeed, from a computational point of view, it is very difficult to handle perimeters, because we are more accustomed to handling functions instead of sets [70, 15], thus replacing the perimeter with a more standard functional involving derivatives of functions allows us to use more robust and more classical numerical methods. We can extend the definition of $\Gamma-$convergence above to families depending on a small real parameter ε. For example, we can treat $\Gamma-$limits of families (F_ε) as $\varepsilon \to 0^+$ [31].

Definition 2.3.2. *We say that a sequence $F_\varepsilon : X \to \mathbb{R}$ $\Gamma-$converges to $F : X \to \mathbb{R}$ as $\varepsilon \to 0^+$ if the following two conditions hold for any $u \in X$.*

1. *(liminf inequality): for every sequence $(u_\varepsilon) \in X$ such that $u_\varepsilon \to u \in X$*

$$F(u) \leq \liminf_{\varepsilon \to 0^+} F_\varepsilon(u_\varepsilon).$$

2. *(limsup inequality): Given $u \in X$, there exists a recovering sequence $(u_\varepsilon) \in X$*

with $u_\varepsilon \to u$ *such that*

$$F(u) \geq \limsup_{\varepsilon \to 0^+} F_\varepsilon(u_\varepsilon).$$

Definition 2.3.3. *(The Modica-Mortola functional) For any* $\varepsilon > 0$*, we consider the following sequence of functionals defined on* $L^1(\Omega)$*,*

$$F_\varepsilon(u) = \begin{cases} \int_\Omega \frac{1}{\varepsilon} W(u) + \varepsilon |\nabla u|^2 dx & \text{if } u \in H^1(\Omega), \\ +\infty & \text{otherwise in } L^1 \end{cases} \tag{2.3.3}$$

where $W : \mathbb{R} \to \mathbb{R}$ *is a double-well potential such that* $W(0) = W(1) = 0$ *and* $W(x) > 0$ *if* $x \notin \{0, 1\}$*. We denote by* c_0 *the constant given by* $c_0 = \int_0^1 \sqrt{W(s)} ds$*. We also define*

$$F(u) = \begin{cases} c_0 Per(A) & \text{if } u = \chi_A \in BV(\Omega), \\ +\infty & \text{otherwise in } L^1 \end{cases} \tag{2.3.4}$$

Theorem 2.3.3. *(Modica-Mortola Theorem) Assume that* Ω *is a bounded convex set. Then* F_ε $\Gamma-$*converges* F *in* $L^1(\Omega)$ *as* $\varepsilon \to 0$*.*

The theorem above (2.3.3) has been proved independently by Sternberg [78] (assuming quadratic growth at ∞).

2.4 Linearized Elasticity

This section contains the analysis of the equations of linearized elasticity that are used to compute the mechanical response of a structure subject to an applied load. Analysis of solid elastic structures using PDEs modeling is one of the major application of modern engineering, which likely makes the PDEs modeling the deformation of elastic

bodies the most popular PDEs in the world. In order to describe the PDEs modeling the deformation of an elastic structure, we first denote the elastic structure as our ground domain Ω with smooth boundary $\partial\Omega$. The domain Ω is subjected to a known traction force f on a part $\Gamma_N \in \partial\Omega$ of its boundary and clamped on $\Gamma_D \in \partial\Omega$.

If u denotes the displacement of the domain Ω due to traction force f acting on Γ_N, then u is governed by the system of equations of linearized elasticity given in strong form below:

$$\begin{cases} -\text{div}\,(\sigma(u)) = 0 \quad \text{in } \Omega, \\ \qquad\qquad u = 0 \quad \text{on } \Gamma_D, \\ \qquad\quad \sigma \cdot n = f \quad \text{on } \Gamma_N, \end{cases} \tag{2.4.1}$$

where $\sigma(u)$ is the stress tensor. Let $\mathrm{e}(u)$ be the linearized strain tensor given by

$$\mathrm{e}(u) = \frac{1}{2}\left(\nabla u + (\nabla u)^T\right) \tag{2.4.2}$$

which can be equivalently written as

$$\mathrm{e}_{ij}(u) = \frac{1}{2}\left(u_{ij} + u_{ji}\right)$$

and

$$\sigma(u) = \mathbb{C}\mathrm{e}(u) \tag{2.4.3}$$

is the *Hooke's law* governing the solid elastic structure and $\mathbb{C}$ is a symmetric stiffness tensor of fourth-order *i.e* a linear map between second-order tensors. For an isotropic homogeneous material, the constitutive equation describing the relationship between

the stress tensor $\sigma(u)$ and linearized strain tensor $\mathrm{e}(u)$ is given as

$$\sigma(u) = \mathbb{C}\mathrm{e}(u) = \lambda \mathrm{tr}(\mathrm{e}(u))I + 2\mu \mathrm{e}(u) \tag{2.4.4}$$

where $\lambda \geq 0, \mu > 0$ are two positive constants, known as *Lamé constants* given by

$$\lambda = \frac{E\nu}{(1+\nu)(1-2\nu)}, \quad \mu = \frac{E}{2(1+\nu)}$$

and E is the *Young's modulus* and ν is the *Poisson ratio.*

2.4.1 Variational Formulation

The linearized elasticity PDE (2.4.1) above can be expressed in *variational* or *weak* formulation. We define the *Sobolev space*

$$V = \{u \in H^1(\Omega) : u = 0 \ \text{ on } \ \Gamma_D\}. \tag{2.4.5}$$

where we will be looking for the *weak solution* of the PDE (2.4.1). The variational formulation of (2.4.1) consists of forming the inner product of

$$-\mathrm{div}\ (\sigma) = 0$$

and a test function $v \in V$ and integrating by parts using *Green's formula* over the domain Ω

$$\int_\Omega -\mathrm{div}\ (\sigma) \cdot v \ dx = \int_\Omega \sigma : \nabla v - \int_{\partial\Omega} (\sigma \cdot n) \cdot v \ ds = 0$$

where the column operator is the inner product between tensors defined as

$$A : B = \sum_{i,j} A_{ij} B_{ij}$$

and n is the outward unit normal at the boundary $\partial\Omega$. Using the boundary conditions of (2.4.1), we obtain the variational formulation of (2.4.1) as

$$\int_\Omega \sigma : \nabla v \, dx = \int_\Omega \mathbb{C}\mathrm{e}(u) : \nabla v \, dx = \int_{\Gamma_N} f \cdot v \, ds \text{ for any } v \in V. \tag{2.4.6}$$

Note that

$$\mathrm{e}(u) : \nabla v = \frac{1}{2} \sum_{i,j} (u_{ij} + u_{ji}) v_{ij} \tag{2.4.7}$$

and since the double summation is over all i and j, the result is unchanged if i and j are interchanged in the summation

$$\mathrm{e}(u) : \nabla v = \frac{1}{2} \sum_{i,j} (u_{ij} + u_{ji}) v_{ji}. \tag{2.4.8}$$

Adding (2.4.7) and (2.4.8), we have

$$\begin{aligned} 2\mathrm{e}(u) : \nabla v &= \frac{1}{2} \sum_{i,j} (u_{ij} + u_{ji}) v_{ij} + \frac{1}{2} \sum_{i,j} (u_{ij} + u_{ji}) v_{ji} \\ &= \frac{1}{2} \sum_{i,j} (u_{ij} + u_{ji})(v_{ij} + v_{ji}) \end{aligned}$$

and therefore

$$\begin{aligned} \mathrm{e}(u) : \nabla v &= \sum_{i,j} \frac{1}{2}(u_{ij} + u_{ji}) \sum_{i,j} \frac{1}{2}(v_{ij} + v_{ji}) \\ &= \mathrm{e}(u) : \mathrm{e}(v) \end{aligned}$$

Replacing ∇v in equation (2.4.6) with the symmetric strain $e(v)$ gives rise to the slightly different variational formulation

$$\int_\Omega \sigma : \mathrm{e}(v)\, dx = \int_\Omega \mathbb{C}\mathrm{e}(u) : \mathrm{e}(v) = \int_{\Gamma_N} f \cdot v\, ds. \tag{2.4.9}$$

We can now summarize the variational formulation as: find $u \in V$ such that

$$a(u, v) = L(v), \ \ \forall v \in V, \tag{2.4.10}$$

where $a : V \times V \to \mathbb{R}$ is a bilinear form

$$a(u, v) = \int_\Omega \mathbb{C}\mathrm{e}(u) : \mathrm{e}(v)\, dx \tag{2.4.11}$$

and $L : V \to \mathbb{R}$ is a linear form

$$L(v) = \int_{\Gamma_N} f \cdot v\, ds. \tag{2.4.12}$$

2.5 Existence of solution

In this section, we show that the linearized elasticity PDE (2.4.1) is well-posed in $H^1(\Omega)$, in the sense that it has a unique solution in $H^1(\Omega)$. The well-possedness of

(2.4.1) is an immediate consequence of classical Lax-Milgram theorem. Before we start the Lax-Milgram theorem, we need some preliminary concepts.

Theorem 2.5.1. *(**Korn's inequality**) Let Ω be a domain in $\mathbb{R}^2$ and let $\Gamma_N \subset \partial\Omega$ be such that length $\Gamma_N > 0$. Then there exists a constant $C_K > 0$ such that*

$$\|\mathrm{e}(u)\|_{L^2(\Omega)} \geq C_K \|u\|_{H^1(\Omega)} \text{ for all } u \in H^1(\Omega).$$

Definition 2.5.1. *Let H denote a real Hilbert space endowed with a inner product $\langle \cdot, \cdot \rangle$ and a norm $\| \cdot \|$. Let $a : H \times H \to \mathbb{R}$ be a bilinear form and $L : H \to \mathbb{R}$ be a linear form. We say that the bilinear form $a(u, v)$ is*

(1) continuous if there exists a constant $M > 0$ such that

$$|a(u, v)| \leq M\|u\|\|v\| \text{ for all } u, v \in H,$$

(2) coercive if there exists a constant $C > 0$ such that

$$a(u, u) \geq C\|u\|^2 \text{ for all } u \in H.$$

Likewise, a linear form $L(v)$ is continuous if there exists a constant $m > 0$ such that

$$|L(v)| \leq m\|v\| \text{ for all } v \in H.$$

Theorem 2.5.2. *(**Cauchy-Schwarz inequality**) If $u, v \in H$, then*

$$|\langle u, v \rangle| \leq \|u\|\|v\|.$$

Theorem 2.5.3. *(**Lax-Milgram theorem**) Let H be a Hilbert space, $a(u,v)$ be a bilinear form on H that is continuous and coercive. Let $L(v)$ be a continuous linear form on H. Then the problem*

$$\textit{Find } u \in H \textit{ such that } a(u,v) = L(v) \textit{ for all } v \in H$$

has a unique solution in H.

Since the linearized elasticity PDE (2.4.1) is equivalent to a variational formulation (2.4.10). It suffices to apply the Lax-Milgram theorem to the variational equation (2.4.10) to show the existence of unique solution. It is easy to see that all the conditions of the Lax-Milgram theorem are satisfied and in particular using the Hilbert space V defined in (2.4.5), the coerciveness of the bilinear form $a(u,v)$ is a direct consequence of Korn's inequality stated in Theorem (2.5.1) combined with the positiveness of the Lamé constants, which together imply that, for all $u \in V$,

$$\begin{aligned} a(u,u) &= \int_\Omega \sigma(u) : \mathrm{e}(u)\, dx \\ &= \int_\Omega (\lambda[\mathrm{tr}(\mathrm{e}(u))]^2 + 2\mu\|\mathrm{e}(u)\|^2)\, dx \\ &\geq \int_\Omega 2\mu\|\mathrm{e}(u)\|^2\, dx \\ &= C\|\mathrm{e}(u)\|_{L^2}^2 \geq C_K\|u\|_V^2. \end{aligned}$$

The continuity of the linear form $L(v)$ is also clear

$$\begin{aligned} |L(v)| &= \left| \int_{\Gamma_N} f \cdot v \, ds \right| \\ &\leq \int_{\Gamma_N} |f \cdot v| \, ds \\ &\leq \|f\|_{L^2(\Gamma_N)} \|v\|_{L^2(\Gamma_N)} \\ &\leq m \|v\|_V \end{aligned}$$

2.6 Responsive optimal design

Consider m responsive linear elastic materials characterized by $(\mathbb{C}_1, \beta_1), \ldots, (\mathbb{C}_m, \beta_m)$ where $\mathbb{C}_i$ denotes the Hooke's law of material i and β_i is a parameter such that $\beta_i = 1$ if material i is responsive and $\beta_i = 0$ otherwise and I_d the $d \times d$ identity matrix. The constitutive laws of these materials depend on an external real valued stimulii set of functions $s_j \in [-1, 1]$ thus, inducing total inelastic strain in dimension d, *i.e*

$$\sigma = \sum_{i}^{m} \mathbb{C}_i \left(\mathrm{e}(u_j) - \beta_i s_j \mathrm{I}_d \right) \tag{2.6.1}$$

where $\mathrm{e}(u_j)$ is the linearized strain associated to a displacement field u_j.

Given a ground domain Ω, let $\Gamma_D \subset \partial\Omega$ be a regular-enough part of the boundary of our domain with non-zero length and $\Gamma_N = \partial\Omega \setminus \Gamma_D$. A design D is a partition of Ω into m subdomains $(D_1, \ldots, D_m)$ occupied by m responsive materials. The problem we are interested in is to design the structure D together with optimal distribution of the stimulii $s = (s_1, s_2, \ldots, s_n)$ that minimizes a general objective function $\mathcal{I}(u_1, u_2, \ldots, u_n)$ where each $u_j \in H^1(\Omega; \mathbb{R})$ is the state variable satisfying

the weak form of the linearized elasticity system

$$\sum_{i=1}^{m} \int_{\Omega} \mathbb{C}_i \left(\mathrm{e}(u_j) - \beta_i s_j \mathrm{I}_d \right) : \mathrm{e}(v)\, dx = 0, \forall v \in V, \tag{2.6.2}$$

where

$$V := \left\{ v \in H^1(\Omega);\, v = 0 \text{ on } \Gamma_D \right\}. \tag{2.6.3}$$

Let $\chi_{D_i}(x)$ be a characteristic function such that

$$\chi_{D_i}(x) = \begin{cases} 1 & x \in D_i,\ i = 1, 2, \ldots, m \\ 0 & x \notin D_i \end{cases} \tag{2.6.4}$$

and define the design variable as

$$\Phi := (\chi_{D_1}, \chi_{D_2}, \ldots, \chi_{D_m}) \tag{2.6.5}$$

such that

$$\sum_{i=1}^{m} \chi_{D_i} = 1, \quad \forall x \in \Omega. \tag{2.6.6}$$

Mathematically, the responsive optimal design problem reads as

$$\begin{cases} \inf\limits_{(\Phi, s) \in \mathcal{D}_\Phi \times \mathcal{S}} \quad \mathcal{I}(u_1, u_2, \ldots, u_n) \\ \\ u_j \text{ satisfies the weak form (2.6.2)} \end{cases} \tag{2.6.7}$$

where $\Phi \in [L^\infty(\Omega; \{0, 1\})]^m$ is the design variable and $\mathcal{S}$ is the space of admissible

stimuli s taking values in $[-1,1]^n$, *i.e*

$$\mathcal{S} = L^1(\Omega : [-1,1]^n). \tag{2.6.8}$$

The space of admissible designs $\mathcal{D}_\Phi$ is given by

$$\mathcal{D}_\Phi = \left\{ \Phi(x) \in [L^\infty(\Omega; \{0,1\})]^m, \int_\Omega \chi_{D_i}\, dx = \theta_i |\Omega| \text{ with } 0 \leq \theta_i \leq 1 \right\} \tag{2.6.9}$$

where θ_i denotes the volume fraction occupied by material i in Ω and

$$\sum_{i=1}^{m} \theta_i = 1. \tag{2.6.10}$$

It is well known that problem (2.6.7) is ill-posed, *i.e*, it admits no optimal solution in the proposed class of admissible designs [5, 16, 29]. This is because the set of feasible designs lacks closure and compactness and in general the infimum can not be attained at any feasible point [29]. This results to so-called checkerboard and mesh-dependency problems. The former refers to the formation of regions of alternating void or holes and solid material ordered in a checkerboard like fashion and is related to the discretization of the original continuous problem. Mesh-dependence concerns the effect that qualitatively different optimal solutions are reached for different mesh-sizes [25]. There are several workaround methods that have been proposed to make problem (2.6.7) well-posed. In the homogenization method [5, 7, 47, 79], the set of admissible designs is expanded to included generalized designs for which one can prove existence of an optimum and derive necessary conditions of optimality. A generalized design is often equivalently called a relaxed, or composite design. This

process of enlarging the space of admissible designs in order to make the problem well-posed is called relaxation [5, 8, 54]. Another workaround is so called Solid Isotropic Microstructure with Penalization (SIMP) introduced by Bendsøe [23]. The idea was to assume continuous densities for the structure as opposed to the discrete form of the homogenization method. Implementing this assumption into topology optimization, the resulting solution can be represented not only with solid and void regions, but with intermediate densities. However, as these are not generally manufacturable, a power-law approach is used to move the intermediate densities towards a 0/1 solution by penalizing the intermediate these densities. The perimeter penalization [16, 50, 66] is another approach to obtain well-posed problem. In this approach, the workaround is to add one extra term to the objective function in order to gain compactness [16, 29]. It has been long understood that adding a surface term proportional to the perimeter of the designs prevents sequences of solutions with rapid oscillations, and makes the problems well posed. In this thesis, we will focus on the perimeter penalization approach. Let

$$\mathcal{P}(\mathrm{D}) := \frac{1}{2}\sum_{i,j=1}^{m} \mathcal{H}^{d-1}\left(\partial^* D_i \cap \partial^* D_j \cap \Omega\right), \tag{2.6.11}$$

where $\mathcal{H}^{d-1}$ denotes the $d-1$–dimensional Hausdorff measure and $\partial^* D$ the essential boundary of a set D. Let $\alpha > 0$ be a small regularization parameter and consider the problem

$$\inf_{(\Phi,s)\in\mathcal{D}_\Phi\times\mathcal{S}} \mathcal{I}(u_1, u_2, \ldots, u_n) + \alpha\mathcal{P}(\mathrm{D}). \tag{2.6.12}$$

2.7 The phase-field approach to optimal design

Numerical implementation of (2.6.12) is very challenging especially the approximation of the perimeter term. The phase-field approach to optimal design, introduced in [28, 29] (see also [83, 86, 82, 81, 84]) is based on the idea of variational approximation of the perimeter penalty term $\mathcal{P}$ for generalized designs. We define a set of *generalized designs*, that is vector-valued functions $\rho \in \mathcal{D}_\rho$, where

$$\mathcal{D}_\rho := \Big\{(\rho_1, \rho_2, \dots, \rho_m) \in \big[H^1(\Omega; [0,1])\big]^m, \int_\Omega \rho_i \, dx = \theta_i |\Omega| \Big\}. \tag{2.7.1}$$

Loosely speaking, the components ρ_i of the vector-valued phase-field ρ can be thought of as a density of material i at each point of the domain Ω, and classical designs would correspond to the situations where $\rho_i = \chi_{D_i}$. Indeed, if $\mathrm{D} \in \mathcal{D}$ is a classical design, then $(\chi_{D_1}, \dots, \chi_{D_m})$ is a generalized design. We then extend $\mathcal{P}$ to generalized designs by defining

$$\mathcal{P}_\varepsilon(\rho) := \int_\Omega \frac{W(\rho)}{\varepsilon} + \varepsilon |D\rho|^2 \, dx, \tag{2.7.2}$$

where $\varepsilon > 0$ is a regularization parameter and W is a non-negative function vanishing only at the vertices $p_1, \dots, p_m$ of the m-dimensional unit simplex and satisfying

$$\inf\left\{ \int_0^1 W^{1/2}(\gamma(t)) |\gamma'(t)| \, dt; \gamma \ \in \ C^1((0,1); \mathbb{R}^m), \gamma(0) \ = \ \rho_i, \gamma(1) \ = \ \rho_j \right\} \ = \ 1.$$

Next, we introduce a convex continuous function a such that $a(0) = 0$ and $a(1) = 1$, so that the equilibrium equation (2.6.2) can then be extended to generalized designs by

$$\sum_{i=1}^m \int_\Omega a(\rho_i) \mathbb{C}_i \left(\mathrm{e}(u_j) - \beta_i s_j \mathrm{I}_d\right) \cdot \mathrm{e}(v) \, dx = 0 \ \forall v \in V. \tag{2.7.3}$$

For a given $\varepsilon > 0$, the phase field regularization of (2.6.12) is then

$$\inf_{(\rho,s)\in\mathcal{D}_\rho\times\mathcal{S}} \mathcal{I}(u_1,\ldots,u_n) + \alpha\mathcal{P}_\varepsilon(\rho). \tag{2.7.4}$$

We show in Chapter 4 in section (4.3) that both problems (2.6.12) and (2.7.4) admit solutions and that the solutions of (2.7.4) converge to that of (2.6.12).

2.8 Adjoint method for sensitivity

In this section, we detail the general procedure for adjoint method. To solve (2.6.12), gradient based optimization is typically employed so one needs to compute the sensitivities of objective function with respect to design changes. These sensitivities are used to update the design with a gradient based optimization method such as conjugate gradient descent, and the process is iterated until convergence tolerance is achieved. To compute these sensitivities by chain's rule, it involves computing the derivative of a state variable with respect to a design variable. Formally, if we consider an objective $F(u(\rho),\rho)$ such that the state variable $u(\rho)$ satisfies the constraint $G(u(\rho),\rho) = 0$, then

$$\frac{dF(u(\rho),\rho)}{d\rho} = \frac{\partial F}{\partial u}\frac{\partial u(\rho)}{\partial \rho} + \frac{\partial F}{\partial \rho}. \tag{2.8.1}$$

To circumvent the computation of the derivative of a state variable with respect to a design variable, we introduce the adjoint method [67, 48]. Starting with an initial design, the linearized elasticity PDE is solved, followed by the adjoint method to obtain the sensitivities. The adjoint method is an efficient way for calculating gradients for constrained optimization problems even for very large dimensional design space [4, 80, 26].

We define the Lagrangian $\mathcal{L}$,

$$\begin{aligned}\mathcal{L}(u_1,\dots,u_n,\rho,s,\lambda_1,\dots,\lambda_n) &= \mathcal{I}(u_1,\dots,u_n)+\alpha\mathcal{P}_\varepsilon(\rho)+\\ &\quad+\underbrace{\sum_{i=1}^{m}\int_\Omega a(\rho_i)\mathbb{C}_i\left(\mathrm{e}(u_j)-\beta_i s\mathrm{I}_2\right)\cdot\mathrm{e}(\lambda_j)}_{=0},\end{aligned}\tag{2.8.2}$$

where each $\lambda_j \in V$ is the Langrange multiplier. Assuming u_j satisfies the equilibrium equation (2.7.3) then the Lagrangian is equivalent to objective function (2.7.4) for any $\lambda_j \in V$ as we have only added zero through the satisfied weak form of equilibrium.

Observe that the solution u_j of the weak formulation (2.7.3) depends on ρ and s so we define a reduced objective function as

$$J(\rho,s) = \mathcal{I}\left(u_1(\rho,s_1),\dots,u_n(\rho,s_n)\right)+\alpha\mathcal{P}_\varepsilon(\rho)$$

and the Lagrangian (2.8.2) becomes

$$\mathcal{L}((u_1(\rho,s_1),\dots,u_n(\rho,s_n),\rho,s,\lambda_1,\dots,\lambda_n) = J(\rho,s).$$

The directional derivative of J on a direction $\tilde{v} \in H^1(\Omega)$ is given as:

$$\begin{aligned}\left\langle \nabla J(\rho,s),\tilde{v}\right\rangle &= \left\langle\frac{\partial\mathcal{L}}{\partial u_1},\frac{\partial u_1}{\partial\rho}\tilde{v}\right\rangle+\dots+\left\langle\frac{\partial\mathcal{L}}{\partial u_n},\frac{\partial u_n}{\partial\rho}\tilde{v}\right\rangle\\ &\quad+\left\langle\frac{\partial\mathcal{L}}{\partial\rho},\tilde{v}\right\rangle+\underbrace{\left\langle\frac{\partial\mathcal{L}}{\partial\lambda_1},\frac{\partial\lambda_1}{\partial\rho}\tilde{v}\right\rangle+\dots+\left\langle\frac{\partial\mathcal{L}}{\partial\lambda_n},\frac{\partial\lambda_n}{\partial\rho}\tilde{v}\right\rangle}_{=0}.\end{aligned}\tag{2.8.3}$$

We choose Lagrange multipliers λ_j such that the last term in equation (2.8.3) disappears since the directional derivative of the Lagrangian function with respect to λ_j

recovers the weak form equillibrium (2.7.3).

Computing $\partial u_j/\partial\rho$ is difficult, so we can choose Lagrange multiplier, λ_j such that for any $v \in V$

$$\left\langle \frac{\partial \mathcal{L}}{\partial u_j}, v \right\rangle = \left\langle \frac{\partial \mathcal{I}}{\partial u_j}, v \right\rangle - \sum_{i=1}^{m} \int_\Omega a(\rho_i)\mathbb{C}_i \mathrm{e}(v) \cdot \mathrm{e}(\lambda_j)\, dx = 0. \tag{2.8.4}$$

Equation (2.8.4) is the weak form of the adjoint equations. After solving (2.8.4) for Lagrange multipliers λ_j, one can find the sensitivity of objective J from

$$\left\langle \nabla J(\rho, s), \tilde{v} \right\rangle = \left\langle \frac{\partial \mathcal{L}}{\partial \rho}, \tilde{v} \right\rangle. \tag{2.8.5}$$

Chapter 3

Responsive minimum compliance with stimulus as design variable

3.1 Problem statement

We briefly recall the classical minimum compliance problem [25] and consider the ground domain Ω in Figure (3.1) to be occupied by three materials *i.e* void, non-responsive and responsive materials.

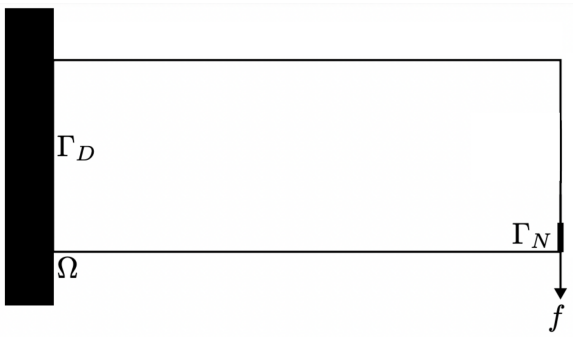

Figure 3.1: Minimum compliace cantiveler beam clamped at Γ_D

We are looking for optimal arrangement of the regions D_1, D_2 and D_3 occupied by void, non-responsive and responsive materials respectively and the distribution of the stimulus s, within the responsive material that minimize the compliance,

$$\mathcal{I}(u) = \int_{\Gamma_N} f \cdot u \, dS. \tag{3.1.1}$$

We consider the regularized minimum compliance problem below,

$$\begin{cases} \min\limits_{(\rho,s)\in\mathcal{D}_\rho\times\mathcal{S}} \mathcal{I}(u) + \alpha\mathcal{P}_\varepsilon(\rho) \\ \\ u \text{ satisfies weak form (4.2.4) with } m = 3 \end{cases} \tag{3.1.2}$$

then we are now ready to prove existence of solutions for the regularized problem. The existence of solutions for the regularized problem (3.1.2) and their convergence to that of the perimeter-controlled topology optimization problem is a relatively straightforward consequence of the now-classical Γ–convergence result for phase transition problems [62, 61, 77, 3]. In [72] section (4.3), we have detailed the proof of existence of solution to a different class of objective function that is continuous function of u. And as in this case, the compliace is continuous function of u, so proof of existence of problem (3.1.2) follows from section (4.3).

3.2 Numerical results

Our implementation uses Firedrake [51, 58], an open source automated system for the solution of partial differential equations in Unified Form Language (UFL) variational

forms [13, 14] using the FEM. The displacement, density, and stimulus fields are discretized using linear Lagrange simplicial finite elements over structured meshes. The minimization algorithm we used is a BNCG (Bounded Nonlinear Conjugate Gradient) solver implemented in the TAO (Toolkit for Advanced Optimization) optimization package, which is a part of PETSc (the Portable, Extensible Toolkit for Scientific Computation) library [18–20]. The numerical implementation of responsive minimum compliance problem follows the staggered algorithm (2). In a *staggered scheme*, we use TAO to minimize the objective function with respect to design only. Whenever computing sensitivity of the objective function with respect to design changes, we perform a full minimization of the objective function with respect to stimulus as outlined in [72] section (4.4).

We present optimal designs for the responsive minimum compliance problem with stimulus in 2D with rectangular domain Ω (see 3.1) with width $L_x = 1.0$ and height $L_y = 1/3$. The domain is clamped on left side and uniform boundary force $f = (0, -1)$ is applied on boundary Γ_N. The regularization parameter is $\varepsilon = 1.0 \times 10^{-4}$ the perimeter penalization parameter is $\alpha = 4.0 \times 10^{-3}$. The relative and absolute tolerance on the gradient and objective function in TAO were set to 1×10^{-7}. The initial design fields are chosen as $\rho_2 = \rho_3 = 0.3$ in Ω. We investigate these final designs for different elastic moduli ratio E_3/E_2 of the responsive to non-responsive material.

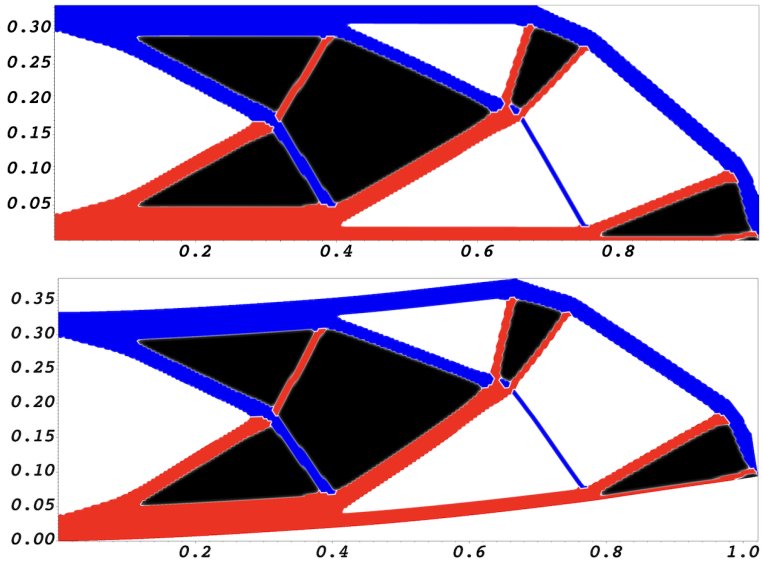

Figure 3.2: Responsive material density (top), non-responsive density (middle) and and composite plot of both material density and the stimulus in the deformed configuration (bottom) for stiffness ratio $E_3/E_2 = 100$. The converged design consists of 30% responsive and 25% non-responsive material.

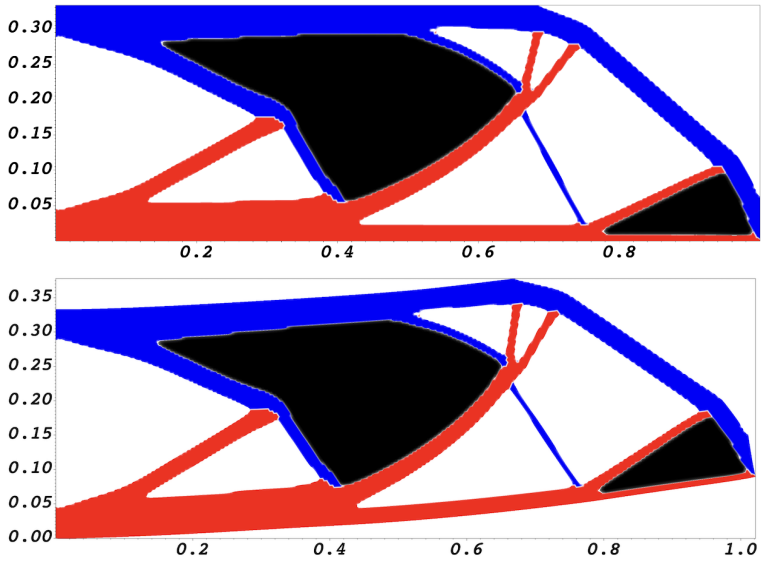

Figure 3.3: Responsive material density (top), non-responsive density (middle) and and composite plot of both material density and the stimulus in the deformed configuration (bottom) for stiffness ratio $E_3/E_2 = 10$. The converged design consists of 25% responsive and 20% non-responsive material.

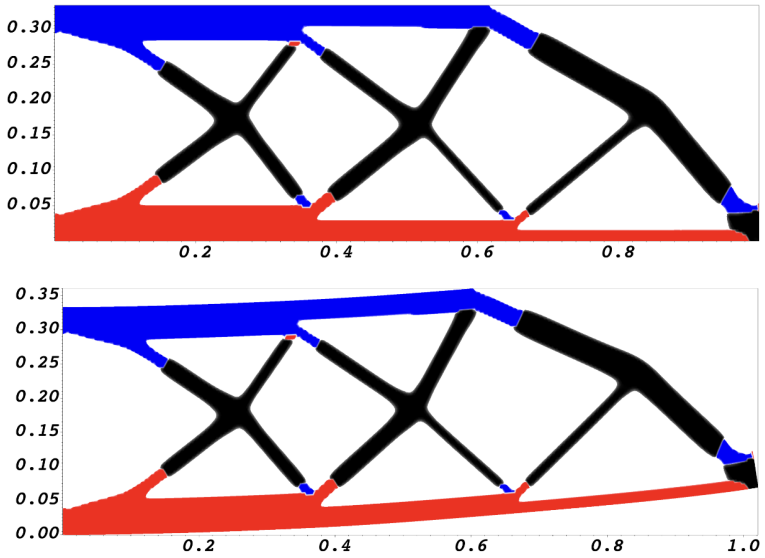

Figure 3.4: Responsive material density (top), non-responsive density (middle) and and composite plot of both material density and the stimulus in the deformed configuration (bottom) for stiffness ratio $E_3/E_2 = 10$. The converged design consists of 16% responsive and 18% non-responsive material.

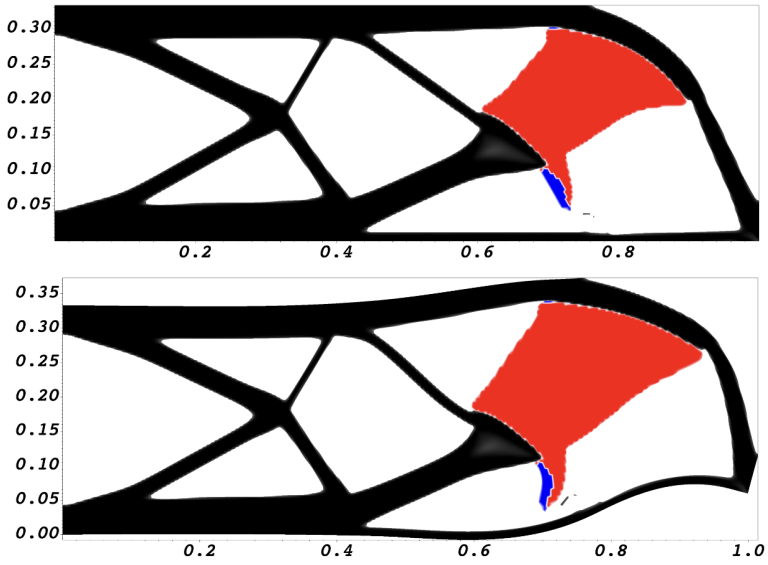

Figure 3.5: Responsive material density (top), non-responsive density (middle) and and composite plot of both material density and the stimulus in the deformed configuration (bottom) for stiffness ratio $E_3/E_2 = 10$. The converged design consists of 12% responsive and 18% non-responsive material

In our first result, Figure (3.2), we consider the responsive material to be 100 stiffer than the non-responsive material. The penalty terms are set to $\nu_3 = 6.0$ and $\nu_2 = -0.02$ for responsive and non-responsive material respectively. Our algorithm converged after 1078 iterations leading to the objective function to decrease from 9.5183 to 0.5481. As expected, final design uses the stiffer material to build the outer frame of the beam. The distribution of the stimulus makes the converged design to act as "bimetallic" strip in sense that, when stimulated the responsive material at the top contracts horizontally while the responsive material at the bottom expands horizontally, causing the beam to do work against the applied load as shown in the last figure in Figure (3.2) above.

In the next Figure (3.3), we consider the responsive material to be 10 stiffer than the non-responsive material. The penalty terms are set to $\nu_3 = 5.0$ and $\nu_2 = 0.38$. As expected, the converged design did not change very much from the that in Figure (3.2) above in a sense that the stronger material is used to build the frame. In this computation, our algorithm converged after 671 iterations leading to the objective function to decrease from 7.1962 to 0.3762.

In our next result, Figure (3.4), we consider the case where responsive and non-responsive materials have the same stiffness. The penalty terms are set to $\nu_3 = 2.0$ and $\nu_2 = 1.0$. The converged design behaves like "bi-metal" strip where the outer layers deform and the shear stiffness of the central area is maximized. Upon stimulation, responsive material at the top contracts while responsive at the bottom expands causing the beam to bend upward as shown in Figure (3.4) below. In this computation, our algorithm converged after 403 iterations leading to the objective function to decrease from 0.57163 to 0.00462.

In the last Figures (3.5) we consider the case where the non-responsive materials is 10 times stiffer than the responsive material. The penalty terms are set to $\nu_3 = 2.0$ and $\nu_2 = 1.0$. As one would expect from the previous results above, we see the converged design uses the stiffer materials to build the frame of the beam and place large chunks of responsive at the bottom. Upon stimulation the converged design behaves similar to (3.4) above. For this computation our algorithm converged after 613 iterations leading to the objective function to decrease from 0.39421 to 0.04932.

3.3 Effect of the perimeter term

The phase-field approach to optimal design uses penalization method to ensure well-posedness of the problem by adding the perimeter term $\alpha\mathcal{P}_\varepsilon(\rho)$ to the objective function where α is an arbitrary penalization parameter or weight of the perimeter. So it is natural to expect that the penalty term or the weight of the perimeter α has significant effect on the final designs. Figure (3.6) shows the effect of decreasing and increasing the weight of the perimeter α while all other parameters are kept as in the previous example. As expected, a larger weight on the perimeter leads to very simple final design whose complexity increases as the weight decreases.

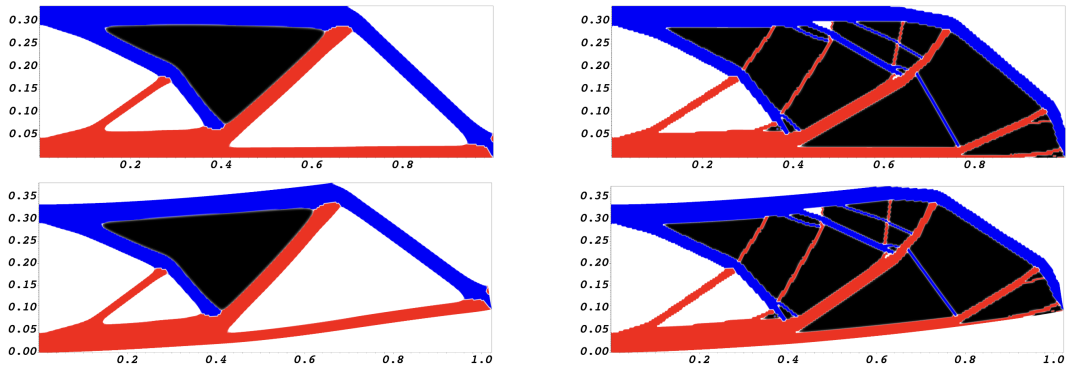

Figure 3.6: Converged design with weight of the perimeter $\alpha = 5.0 \times 10^{-2}$(left) and $\alpha = 5.0 \times 10^{-4}$(right).

3.4 Influence of initial design

We observe that different initial design guesses may lead to different converged designs but the actual converged values of the objective function remain very close. This is

due to non-convexity nature of our minimization problem. Figure (3.7) shows a connverged design for initial design as given as

$$\rho_2 = 0.5 + 0.5\sin(4\pi x)\sin(8\pi y),$$
$$\rho_3 = 0.3 + 0.3\cos(4\pi x)\cos(8\pi y).$$

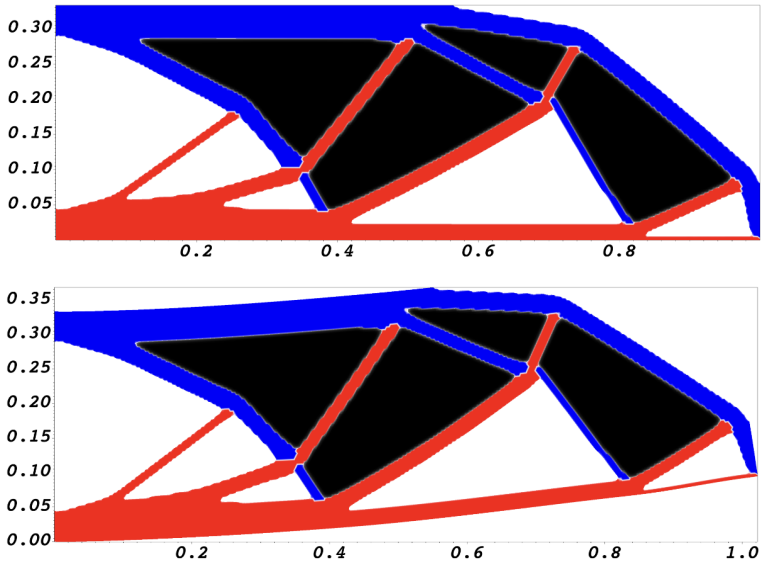

Figure 3.7: Converged design with different initial design guess.

3.5 Conclusion

Through the responsive minimum compliance example, we introduced the *staggered* scheme which produced expected results in classical compliance problem. Due to

ill-posedness of the minimum compliance problem, we discussed the methods to regularize the design problem to gain well-posedness. In particular, we detailed the perimeter penalization, where a perimeter term is added to the objective function and the proof of existence of minimizers follows from classical $\Gamma-$ocnvergence. Our staggered scheme exhibits good robustness properties upon mesh refnement or changes of initial design. Even though, it can produce slightly diferent designs for diferent initial designs, which is common in due to non-convex nature of optimization problem, but the objective value of the computed designs are very close. We also demonstrated the effect of a perimeter term on complexity of the design which is common in phase-field models.

Chapter 4

Systematic design of compliant morphing structures with stimulus as design variable

Advances in additive manufacturing and synthesis of complex "responsive" materials whose properties can be altered through external stimuli are opening the door to a new generation of integrated devices and materials. While manufacturing such structures or materials has received a considerable attention (see for instance [71, 85]), their actual design is equally challenging. Starting from the pioneering work of [73, 56, 52, 44, 74, 75], topology optimization has established itself as a powerful tool for systematic design of micro-devices, MEMS, or materials microstructures. In such problem, the distribution of one or several materials in a ground domain that optimizes an objective function is sought algorithmically [25]. It is well-known that such problems are generally ill-posed (see [5] for instance) with optimal designs consisting of a fine mixture of multiple materials. Homogenization approaches [35, 8, 5] tackle

this problem directly by extending admissible designs to such mixtures. This type of approach is mathematically well grounded and leads to well posed problems that can be implemented efficiently. However, it is often criticized for leading to designs that cannot be manufactured. Several other classes of techniques aim at restricting the class of admissible designs in such a way that avoids fine mixtures. The combination of material interpolation (SIMP) and filters [21, 27] is a commonly employed approach. Shape parameterization by level set functions [10, 12] also limits the complexity of designs. Finally, by penalizing the length (or surface) of interfaces between materials, perimeter penalization [16, 50, 66] also produces designs with limited complexity. Additionally, perimeter penalization can be efficiently implemented using a phase-field approach [28, 29, 82].

In this article, we propose a phase-field algorithm for the systematic design of responsive structures achieving prescribed deformations under some unknown distributions of a stimulus. Our focus is on linear elastic materials in which an external stimulus can generate an isotropic inelastic strain, similar to linear thermo-elastic materials.

Section(4.1) is devoted to the mathematical analysis of the problem and its phase-field approximation. A numerical scheme is proposed in Section(4.4) and illustrated by a series of numerical simulations in Section(4.5).

4.1 Problem statement

Consider linear elastic materials whose constitutive laws depend on an external real-valued stimulus $s \in [-1, 1]$ inducing an inelastic strain in dimension d, *i.e.*

$$\sigma = \mathbb{C}\left(\mathrm{e}(u) - \beta s \mathrm{I}_d\right) \tag{4.1.1}$$

where $\mathbb{C}$ denotes the Hooke's law, $\mathrm{e}(u) = (\nabla u + \nabla u^T)/2$ is the linearized strain associated to a displacement field u, $\beta \geq 0$ is a given parameter and I_d the $d \times d$ identity matrix. Throughout this article, we call such a material a *responsive material* characterized by $\mathbb{C}$ and β.

Consider a bounded open domain $\Omega \subset \mathbb{R}^d$, $d = 2, 3$, and an open subset Ω_0 of Ω. A *design* D is a partition of Ω into m subdomains $(D_1, \ldots, D_m)$ occupied by m responsive materials characterized by $(\mathbb{C}_1, \beta_1), \ldots, (\mathbb{C}_m, \beta_m)$. Let $\Gamma_D \subset \partial\Omega$ be a regular-enough part of the boundary of our domain with non-zero length and $\Gamma_N = \partial\Omega \backslash \Gamma_D$. Consider n prescribed displacement fields $(\bar{u}_1, \ldots, \bar{u}_n) \in \left[H^1(\Omega_0; \mathbb{R}^d)\right]^n$ defined over Ω_0. Our goal is to design a structure D and a family of stimulus functions $\mathrm{s} := (s_1, \ldots, s_n)$ such that in the equilibrium configuration associated with each stimuli stimulus s_j, Ω_0 is mapped to a region as close as possible to $\bar{u}_j(\Omega_0)$, $j = 1, \ldots, n$. More precisely, let $(\theta_1, \ldots, \theta_m)$ such that $\sum_{i=1}^m \theta_i = 1$ be a set of prescribed volume fractions in $[0, 1]$, and let Ω_0 be an open subset of Ω. The space of admissible designs consists of partition

of Ω in subsets with prescribed volume fraction, *i.e.*

$$\mathcal{D} := \Big\{(D_1, \dots, D_m);\ \bigcup_{1\le j\le m} \bar{D}_i = \Omega,\ D_i \cap D_j = \emptyset\ 1 \le i < j \le m, \\ |D_i| = \theta_i|\Omega|,\ i = 1, \dots, m\Big\}. \quad (4.1.2)$$

We consider the space of admissible stimuli s taking values in $[-1, 1]^n$, *i.e.*

$$\mathcal{S} := L^1\left(\Omega, [-1, 1]^n\right). \quad (4.1.3)$$

Given a design D and a set of stimuli s, we define

$$\mathcal{I}(u_1, \dots, u_n) := \sum_{j=1}^{n} \frac{1}{2} \int_{\Omega_0} |u_j(x) - \bar{u}_j(x)|^2 \, dx, \quad (4.1.4)$$

where the $u_j \in V$, $1 \le j \le n$, satisfy the weak form of the linearized elasticity system

$$\sum_{i=1}^{m} \int_{\Omega} \mathbb{C}_i \left(\mathrm{e}(u_j) - \beta_i s_j \mathrm{I}_d\right) \cdot \mathrm{e}(\phi) \, dx = 0, \forall \phi \in V, \quad (4.1.5)$$

where

$$V := \left\{\phi \in H^1(\Omega);\ \phi = 0 \text{ on } \Gamma_D\right\}. \quad (4.1.6)$$

It is well-know that minimizing $\mathcal{I}$ with respect to designs is an ill-posed problem, which leads to significant numerical issues such as mesh-dependent solutions and "checkerboards". Typical workaround consist in considering generalized domains as in homogenization approaches [8, 5], or the use of material interpolation laws [25] and "filters" [73, 27]. Level set-based approaches [10, 12], which *de facto* impose restrictions on the topology of the admissible designs are also known to address these

issues. Perimeter penalization [16, 50, 66] is another approach to obtain well-posed problem. Let

$$\mathcal{P}(\mathrm{D}) := \frac{1}{2}\sum_{i,j=1}^{m} \mathcal{H}^{d-1}\left(\partial^* D_i \cap \partial^* D_j \cap \Omega\right), \tag{4.1.7}$$

where $\mathcal{H}^{d-1}$ denotes the $d-1$–dimensional Hausdorff measure and $\partial^* D$ the essential boundary of a set D (see [17] Definition 3.60). Let $\alpha > 0$ be a small regularization parameter and consider the problem

$$\inf_{(\mathrm{D},\mathrm{s})\in\mathcal{D}\times\mathcal{S}} \mathcal{I}(u_1,\ldots,u_n) + \alpha\mathcal{P}(\mathrm{D}). \tag{4.1.8}$$

4.2 Phase-field regularization

The phase-field approach to optimal design, introduced in [28, 29] (see also [83, 86, 82, 65]) is based on the idea of variational approximation of the perimeter penalty term $\mathcal{P}$ for generalized designs. We define a set of *generalized designs*, that is vector-valued functions $\rho \in \mathcal{D}_\rho$, where

$$\mathcal{D}_\rho := \Big\{(\rho_1,\rho_2,\ldots,\rho_m) \in \left[H^1(\Omega;[0,1])\right]^m, \\ \sum_{i=1}^{m}\rho_i = 1, \int_\Omega \rho_i\,dx = \theta_i|\Omega|,\ 1\le i\le m\Big\}. \tag{4.2.1}$$

Loosely speaking, the components ρ_i of the vector-valued phase-field ρ can be thought of as a density of material i at each point of the domain Ω, and classical designs would correspond to the situations where $\rho_i = \chi_{D_i}$. Indeed, if $\mathrm{D}\in\mathcal{D}$ is a classical design, then $(\chi_{D_1},\ldots,\chi_{D_m})$ is a generalized design. We then extend $\mathcal{P}$ to generalized designs

by defining

$$\mathcal{P}_\varepsilon(\rho) := \int_\Omega \frac{W(\rho)}{\varepsilon} + \varepsilon |D\rho|^2 \, dx, \tag{4.2.2}$$

where $\varepsilon > 0$ is a regularization parameter and W is a non-negative function vanishing only at the vertices $p_1, \ldots, p_m$ of the m-dimensional unit simplex and satisfying

$$d_{ij} := \inf\left\{ \int_0^1 W^{1/2}(\gamma(t)) |\gamma'(t)| \, dt; \gamma \in C^1((0,1); \mathbb{R}^m), \gamma(0) = \rho_i, \gamma(1) = \rho_j \right\} = 1 \tag{4.2.3}$$

for all $1 \leq i < j \leq m$.

Next, we introduce a convex continuous function a such that $a(0) = 0$ and $a(1) = 1$, so that the equilibrium equation (4.1.5) can then be extended to generalized designs by

$$\sum_{i=1}^m \int_\Omega a(\rho_i) \mathbb{C}_i \left(\mathrm{e}(u_j) - \beta_i s_j \mathrm{I}_d \right) \cdot \mathrm{e}(\phi) \, dx = 0 \ \forall \phi \in V, \ 1 \leq j \leq n. \tag{4.2.4}$$

For a given $\varepsilon > 0$, the phase field regularization of (4.1.8) is then

$$\inf_{(\rho,\mathrm{s}) \in \mathcal{D}_\rho \times \mathcal{S}} \mathcal{I}(u_1, \ldots, u_n) + \alpha \mathcal{P}_\varepsilon(\rho). \tag{4.2.5}$$

We show in the next Section that both problems admit solutions and that the solutions of (4.1.8) converge in some sense to that of (4.2.5). This result justifies numerical approach presented below and which consists in minimizing (4.2.5) for "small" values of the regularization parameter ε.

4.3 Existence of solutions

The existence of minimizers for the regularized problem (4.2.5) and their convergence to that of the perimeter-controlled topology optimization problem (4.1.8) is a relatively straightforward consequence of the now-classical Γ–convergence result for phase transition problems [62, 61, 77, 3].

Prior to stating our main result, we need to introduce a few notations. Let

$$\widetilde{\mathcal{P}}_\varepsilon(\rho, \mathrm{s}) := \begin{cases} \mathcal{P}_\varepsilon(\rho) & \text{if } (p, \mathrm{s}) \in \mathcal{D}_\rho \times \mathcal{S} \\ +\infty & \text{otherwise,} \end{cases} \tag{4.3.1}$$

and

$$\widetilde{\mathcal{P}}(\rho, \mathrm{s}) := \begin{cases} \mathcal{P}(\rho) & \text{if } (p, \mathrm{s}) \in \widetilde{\mathcal{D}} \times \mathcal{S} \\ +\infty & \text{otherwise,} \end{cases} \tag{4.3.2}$$

where

$$\widetilde{\mathcal{D}} = \{\rho; \exists (D_1, \ldots, D_m) \in \mathcal{D}, \rho_i = \chi_{D_i},\ 1 \leq i \leq n\}, \tag{4.3.3}$$

and

$$\widetilde{\mathcal{I}}(\rho, \mathrm{s}) = \mathcal{I}\left(u_1(\rho, s_1), \ldots, u_n(\rho, s_n)\right), \tag{4.3.4}$$

where $u_j(\rho)$, $1 \leq j \leq n$ satisfy (4.2.4). We are now able to state the main existence and approximation result:

Theorem 4.3.1. *For any given $\varepsilon > 0$, the problem*

$$\inf_{(\rho, \mathrm{s}) \in \mathcal{D}_\rho \times \mathcal{S}} \widetilde{\mathcal{I}}(\rho, \mathrm{s}) + \alpha \widetilde{\mathcal{P}}_\varepsilon(\rho, \mathrm{s}), \tag{4.3.5}$$

admits a solution $(\rho_\varepsilon, \mathrm{s}_\varepsilon)$. *Furthermore, there exists* $(\rho, s) \in \widetilde{\mathcal{D}} \times \mathcal{S}$ *such that* $\rho_{\varepsilon'} \to \rho$ *in* $[L^1(\Omega)]^m$ *and* $\mathrm{s}_{\varepsilon'} \rightharpoonup \mathrm{s}$ *in* $[L^p(\Omega)]^n$ *for any* $1 < p \leq \infty$ *and* ρ *is a solution of*

$$\inf_{(\rho,\mathrm{s})\in\mathcal{D}_\rho\times\mathcal{S}} \widetilde{\mathcal{I}}(\rho,\mathrm{s}) + \alpha\widetilde{\mathcal{P}}(\rho,\mathrm{s}). \tag{4.3.6}$$

Before proving Theorem 4.3.1, we state and prove several preliminary lemmas.

Lemma 4.3.2 (Equi-coercivity of the displacements)**.** *Let* $(\rho, \mathrm{s}) \in \mathcal{D}\times\mathcal{S}$ *and* $k_1, k_2, k_3 > 0$ *be such that for any* $1 \leq i \leq m$ *and for any* $\Psi \in \mathrm{M}^{d\times d}_{\mathrm{sym}}$

$$k_1\Psi\cdot\Psi \leq \mathbb{C}_i\Psi\cdot\Psi \leq k_2\Psi\cdot\Psi, \tag{4.3.7}$$

and for any $1 \leq j \leq n$,

$$|\beta_i| \leq k_3. \tag{4.3.8}$$

There exists $C > 0$ *such that if* $(u_1, \dots u_n) \in V^n$ *satisfies* (4.2.4)*, then*

$$\|u_j\|_{H^1(\Omega)} \leq C,\ 1 \leq j \leq n.$$

Proof. Using u_j as the test function in (4.2.4), we obtain

$$\int_\Omega \sum_{i=1}^m a(\rho_i)\mathbb{C}_i\mathrm{e}(u)\cdot\mathrm{e}(u)\,dx = \int_\Omega \sum_{i=1}^m a(\rho_i)\beta_i s\mathbb{C}_i\mathrm{e}(u)\cdot\mathrm{I}_d\,dx.$$

Using then (4.3.7), and Cauchy-Schwarz inequality, we get

$$k_1\sum_{i=1}^m a(\rho_i)\|\mathrm{e}(u)\|^2_{L^2(\Omega)} \leq \|\mathrm{e}(u)\|_{L^2(\Omega)}\left\|\sum_{i=1}^m a(\rho_i)\beta_i\mathbb{C}_i\mathrm{I}_d\right\|_{L^2(\Omega)}.$$

Since a is convex on $[0,1]$, $0 \leq \rho_i \leq 1$, and $\sum_i \rho_i = 1$ we have

$$\sum_{i=1}^{m} a(\rho_i) \geq a\left(\sum_{i=1}^{m} \rho_i\right) = a(1) = 1.$$

Furthermore, since $a(\rho_i) < 1$ for all i, we conclude that

$$k_1 \|\mathrm{e}(u)\|^2_{L^2(\Omega)} \leq k_3 \|\mathrm{e}(u)\|_{L^2(\Omega)} \left\| \sum_{i=1}^{m} \mathbb{C}_i \mathrm{I}_d \right\|_{L^2(\Omega)},$$

hence that

$$k_1 \|\mathrm{e}(u)\|_{L^2(\Omega)} \leq C,$$

for some $C > 0$. We then conclude using Korn's inequality with boundary conditions [37, Theorem 6.15-4]. □

Lemma 4.3.3 (Continuity of displacements)**.** *Let $\mathbb{C}_i$, β_i be as in Lemma 4.3.2. Consider a sequence $(\rho_\varepsilon, \mathrm{s}_\varepsilon)_\varepsilon \in \mathcal{D}_\rho \times S$ of designs and stimuli and $(\rho, s) \in \widetilde{\mathcal{D}} \times \mathcal{S}$ be such that $\rho_\varepsilon \to \rho$, in $[L^1(\Omega)]^m$ and $\mathrm{s}_\varepsilon \rightharpoonup \mathrm{s}$ in $[L^2(\Omega)]^n$. Let $u_\varepsilon = (u_{1,\varepsilon}, \ldots, u_{n,\varepsilon})$ (resp. $u = (u_1, \ldots, u_n)$) be the equilibrium displacements associated with $(\rho_\varepsilon, \mathrm{s}_\varepsilon)$ (resp. (ρ, s)), given by (4.2.4) (resp. (4.1.5)). Then if the $\mathbb{C}_i$ and β_i satisfy the hypotheses of Lemma 4.3.2, $u_\varepsilon \to u$ in $[L^2(\Omega)]^n$.*

Proof. Note first that using Lemma 4.3.2, we have that the sequence $(u_\varepsilon)_\varepsilon$ is uniformly bounded in $[H^1(\Omega)]^n$ so that there exists $u^* \in V^n$ such that $u_\varepsilon \rightharpoonup u^*$ in $[H^1(\Omega)]^n$. We need to show that u^* satisfies (4.1.5) from which we will deduce that $u^* = u$.

Given any $1 \leq j \leq n$, let $\psi \in C^0_c(\Omega, \mathrm{M}^{d\times d}_{\mathrm{sym}})$ be a test function. Denoting $\rho_{i,\varepsilon}$,

$1 \leq i \leq m$, the components of ρ_ε, we have that

$$\left| \int_\Omega \sum_{i=1}^m \left[a(\rho_{i,\varepsilon}) \mathbb{C}_i \left(\mathrm{e}(u_{j,\varepsilon}) - \beta_i s_{j,\varepsilon} \mathrm{I}_d \right) - a(\rho_i) \mathbb{C}_i \left(\mathrm{e}(u^*) - \beta_i s \mathrm{I}_d \right) \right] \cdot \psi \, dx \right| \leq$$
$$\left| \int_\Omega \sum_{i=1}^m \left[\left(a(\rho_{i,\varepsilon}) - a(\rho_i) \right) \mathbb{C}_i \left(\mathrm{e}(u_{j,\varepsilon}) - \beta_i s_{j,\varepsilon} \mathrm{I}_d \right) \right] \cdot \psi \, dx \right|$$
$$+ \left| \int_\Omega \sum_{i=1}^m \left[a(\rho_i) \mathbb{C}_i \left(\mathrm{e}(u_{j,\varepsilon}) - \mathrm{e}(u^*) - \beta_i s_{j,\varepsilon} \mathrm{I}_d + \beta_i s \mathrm{I}_d \right) \right] \cdot \psi \, dx \right|. \quad (4.3.9)$$

Since $|\beta_i| \leq k_3$, $u_{j,\varepsilon} \rightharpoonup u_j^*$ in $H^1(\Omega)$, and $s_{j,\varepsilon} \rightharpoonup s_j$ in $L^2(\Omega)$, the second term in the right-hand side of (4.3.9) converges to 0. We then write

$$\left| \int_\Omega \sum_{i=1}^m \left[\left(a(\rho_{i,\varepsilon}) - a(\rho_i) \right) \mathbb{C}_i \left(\mathrm{e}(u_{j,\varepsilon}) - \beta_i s_{j,\varepsilon} \mathrm{I}_d \right) \right] \cdot \psi \, dx \right|$$
$$\leq \sum_{i=1}^m \left\| \left(a(\rho_{i,\varepsilon}) - a(\rho_i) \right) \psi \right\|_{L^2(\Omega)} \left\| \mathbb{C}_i \left(\mathrm{e}(u_{j,\varepsilon}) - \beta_i s_{j,\varepsilon} \mathrm{I}_d \right) \right\|_{L^2(\Omega)}$$
$$\leq k_2 \sum_{i=1}^m \left\| \left(a(\rho_{i,\varepsilon}) - a(\rho_i) \right) \psi \right\|_{L^2(\Omega)} \left\| \mathrm{e}(u_{j,\varepsilon}) - \beta_i s_{j,\varepsilon} \mathrm{I}_d \right\|_{L^2(\Omega)},$$

and since $\rho_\varepsilon \to \rho$ in L^1 and is uniformly bounded in $L^\infty(\Omega)$, we get that $\left\| \left(a(\rho_{i,\varepsilon}) - a(\rho_i) \right) \psi \right\|_{L^2(\Omega)} \to 0$ for any $1 \leq i \leq m$. Using then Lemma 4.3.2, we get that $\mathrm{e}(u_{j,\varepsilon})$ is uniformly bounded in $L^2(\Omega)$. Since s_ε is uniformly bounded in $L^\infty(\Omega)$ hence in $L^2(\Omega)$, the first term in the right-hand side of (4.3.9) also converges to 0. Finally, by density of C_c^0 in L^2 we get that for any $\phi \in V$, $\left| \int_\Omega \left(a(\rho_{i,\varepsilon}) - a(\rho_i) \right) \mathbb{C}_i \left(\mathrm{e}(u_{j,\varepsilon}) - \beta_i s_{j,\varepsilon} \mathrm{I}_d \right) \cdot \mathrm{e}(\phi) \, dx \right| \to 0$ and leveraging (4.1.5) that for any $\in V$ and $1 \leq i \leq m$:

$$\int_\Omega \sum_{i=1}^m a(\rho_i) \mathbb{C}_i \left(\mathrm{e}(u_j^*) - \beta_i s_j \mathrm{I}_d \right) \cdot \mathrm{e}(\phi) \, dx = 0,$$

i.e. that $u^* = u$ solves (4.1.5). □

Lemma 4.3.4 (Compactness)**.** *Let $(\rho_\varepsilon, \mathrm{s}_\varepsilon) \in \mathcal{D}_\rho \times \mathcal{S}$ and the associated equilibrium displacements $u_{j,\varepsilon}$, $1 \leq j \leq n$ be such that $\mathcal{I}(u_{1,\varepsilon}, \dots, u_{n,\varepsilon}) + \alpha\widetilde{\mathcal{P}}_\varepsilon(\rho_\varepsilon, \mathrm{s}_\varepsilon)$ is uniformly bounded. Then there exists a subsequence $(\rho_\varepsilon, \mathrm{s}_\varepsilon)_{\varepsilon'} \subset (\rho_\varepsilon, \mathrm{s}_\varepsilon)_\varepsilon$ and $(\rho, \mathrm{s}) \in \widetilde{\mathcal{D}} \times \mathcal{S}$ such that $\rho_{\varepsilon'} \to \rho$ in $[L^1(\Omega)]^m$ and $\mathrm{s}_{\varepsilon'} \rightharpoonup \mathrm{s}$ in $[L^p(\Omega)]^n$ for any $1 < p \leq \infty$.*

Proof. The compactness of the designs ρ_ε derives directly from the compactness theorem for $\mathcal{P}_\varepsilon$ [77, Proposition 4.1], whereas that of the stimuli s_ε derives from the uniform L^∞ bound on stimuli in the definition of $\mathcal{S}$.

□

Remark 1. *Note that $\mathcal{D}_\rho$ is a convex closed subset of H^1 and hence it is closed under weak convergence, so that when we extract a subsequence of designs, it remains in $\mathcal{D}_\rho$ and its limit is also in $\mathcal{D}_\rho$.*

Proof of Theorem 4.3.1. Having proved the lemma, the proof of Theorem 4.3.1 is straightforward. Note first that from [77, Theorem 2.5], we have that $\widetilde{\mathcal{P}}_\varepsilon \xrightarrow{\Gamma(L^1)} \widetilde{\mathcal{P}}$. From Lemma 4.3.3, we get that $\widetilde{\mathcal{I}}$ is a continuous function of ρ, s, so that by stability of Γ–convergence by continuous perturbations, we get that for any $\alpha > 0$ $\widetilde{\mathcal{I}} + \alpha\widetilde{\mathcal{P}}_\varepsilon$ Γ–converges to $\widetilde{\mathcal{I}} + \alpha\widetilde{\mathcal{P}}$ for the $[L^1(\Omega)]^m$ strong times $[L^p(\Omega)]^n$ weak topology for any $1 < p \leq \infty$. Secondly, from the compactness and continuity lemmas 4.3.2 and 4.3.3, and the equi-coercivity and lower semiconinuity of $\mathcal{P}_\varepsilon$ ([77, Proposition 4.1]), we get that $\widetilde{\mathcal{I}} + \alpha\widetilde{\mathcal{P}}$ admits minimizers for any $\varepsilon > 0$ and that the minimizing sequence is compact. We can then conclude the proof of Theorem 4.3.1 by a direct application of the fundamental theorem of Γ–convergence. □

Remark 2. *Note that the hypotheses of Lemma 4.3.2 rule out a degenerate Hooke's law $\mathbb{C} = 0$ for any of the materials (*i.e. *optimizing the distribution of $m-1$ materials*

with the m^{th} materials playing the role of "void"). As is common practice, in this situation we we introduce an artificial stiffness parameter η and replace the "void" phase with a weak material with Hooke's law $\eta\mathrm{I}$. Taking the limit as $\eta \to 0$ is technical (see for instance [28, Section 4]), and we did not attempt to study this limit here.

4.4 Numerical implementation

In all that follows, we focus on the spacial case of three materials, "void", a non-responsive material, and a responsive material with density ρ_1, ρ_2 and ρ_3 respectively. For the "void" and non-responsive materials, we set $\beta_1 = \beta_2 = 0$ in (4.2.4) whereas up to a change of scale, we can choose $\beta_3 = 1$ without loss of generality.

We handle the constraint $\rho_1+\rho_2+\rho_3 = 1$ explicitly by substituting $\rho_1 = 1-\rho_2-\rho_3$ and optimizing with respect to $\tilde{\rho} = (\rho_2, \rho_3)$ under the constraint $0 \leq \rho_2, \rho_3 \leq 1$. Of course, this means that ρ_1 only satisfies $-1 \leq \rho_1 \leq 1$. However, it is easy to see that the proof of Theorem 4.3.1 still holds in this case, provided that a be extended to $[-1, 1]$ as an even function. With an abuse of notation, we write $\mathcal{I}(\tilde{\rho}, \mathrm{s})$ and $\mathcal{P}_\varepsilon(\tilde{\rho}, \mathrm{s})$ to denote $\mathcal{I}((1-\rho_2-\rho_3, \rho_2, \rho_3), \mathrm{s})$ and $\mathcal{P}_\varepsilon((1-\rho_2-\rho_3, \rho_2, \rho_3), \mathrm{s})$ respectively.

It is then natural to enforce null-stimulus in materials 1 and 2, which is easily achieved by adding a penalty term of the form

$$Q(\tilde{\rho}, \mathrm{s}) = \int_\Omega ((1-\rho_2-\rho_3)^2 + \rho_2^2) \sum_{j=1}^{n} s_j^2 \, dx \tag{4.4.1}$$

to the objective function.

Similarly, instead of enforcing the volume fraction constraints $\int_\Omega \rho_i \, dx = \theta_i |\Omega|$,

$i = 2, 3$ strongly, we introduce a penalty term

$$V_C(\tilde{\rho}) = \nu_2 \int_\Omega \rho_2 \, dx + \nu_3 \int_\Omega \rho_3 \, dx, \tag{4.4.2}$$

where ν_2 and ν_3 are two penalty factors set by trial and error.

With these changes, our problem becomes

$$\inf_{(\tilde{\rho},\mathrm{s})\in[H^1(\Omega;[0,1])]^2\times\mathcal{S}} \mathcal{O}(\tilde{\rho},\mathrm{s}) \quad := \quad \widetilde{\mathcal{I}}(\tilde{\rho},\mathrm{s}) \; + \; \alpha\mathcal{P}_\varepsilon(\tilde{\rho}) \; + \; V_C(\tilde{\rho}) \; + \; Q(\tilde{\rho},\mathrm{s}). \tag{4.4.3}$$

4.4.1 Sensitivity analysis

Given an admissible pair of design variables $(\rho, \mathrm{s}) \in \mathcal{D}_\rho \times \mathcal{S}$ and $(u_1, \ldots, u_n) \in V^n$ admissible displacement fields, we define the Lagrangian $\mathcal{L}$

$$\mathcal{L}(u_1, \ldots, u_n, \tilde{\rho}, \mathrm{s}, \lambda_1, \ldots, \lambda_n) = \mathcal{O}(\tilde{\rho}, \mathrm{s}) + \sum_{j=1}^{n} \sum_{i=1}^{3} \int_\Omega a(\rho_i)\mathbb{C}_i \left(\mathrm{e}(u_j) - \beta_i s_j \mathrm{I}_d\right) \cdot \mathrm{e}(\lambda_j) \, dx, \tag{4.4.4}$$

where $(\lambda_1, \ldots \lambda_n) \in V^n$ are Lagrange multipliers.

Let $(u_1(\tilde{\rho}, s_1), \ldots, u_n(\tilde{\rho}, s_n))$ be the equilibrium displacements associated to $(\tilde{\rho}, \mathrm{s})$ satisfying (4.2.4) and define

$$J(\tilde{\rho}, \mathrm{s}) = \mathcal{O}\left(u_1(\tilde{\rho}, s_1), \ldots, u_n(\tilde{\rho}, s_n)\right).$$

so that

$$\mathcal{L}(u_1(\tilde{\rho}, s_1), \ldots, u_n(\tilde{\rho}, s_n), \tilde{\rho}, s, \lambda_1, \ldots, \lambda_n) = J(\tilde{\rho}, \mathrm{s}).$$

Formally, the directional derivative of J in a direction $\phi \in [H^1(\Omega)]^2$ is given by:

$$\left\langle \frac{\partial J}{\partial \tilde{\rho}}, \phi \right\rangle \quad = \quad \left\langle \frac{\partial \mathcal{L}}{\partial u_1}, \frac{\partial u_1}{\partial \tilde{\rho}}\phi \right\rangle \; + \; \cdots \; + \; \left\langle \frac{\partial \mathcal{L}}{\partial u_n}, \frac{\partial u_n}{\partial \tilde{\rho}}\phi \right\rangle \; + \; \left\langle \frac{\partial \mathcal{L}}{\partial \tilde{\rho}}, \phi \right\rangle. \quad (4.4.5)$$

As is customary, instead of computing $\partial u_j/\partial\tilde{\rho}$, we choose Lagrange multipliers, $\lambda_1^*, \ldots \lambda_n^*$ satisfying the adjoint equations:

$$\left\langle \frac{\partial \mathcal{L}}{\partial u_j}, v \right\rangle = \int_{\Omega_0} (u_j - \bar{u}_j) v \, dx - \sum_{i=1}^{3} \int_{\Omega} a(\rho_i) \mathbb{C}_i \mathrm{e}(\lambda_j^*) \cdot \mathrm{e}(v) \, dx = 0, \; 1 \le j \le n. \quad (4.4.6)$$

for any $v \in V$. With this choice of Lagrange multipliers, we get

$$\left\langle \frac{\partial J}{\partial \tilde{\rho}}(\tilde{\rho}, s), \phi \right\rangle = \left\langle \frac{\partial \mathcal{L}}{\partial \tilde{\rho}}(u_1(\tilde{\rho}, s_1), \ldots, u_n(\tilde{\rho}, s_n), \tilde{\rho}, \mathrm{s}, \lambda_1^*, \ldots \lambda_n^*), \phi \right\rangle,$$

i.e.,

$$\begin{aligned} \left\langle \frac{\partial J}{\partial \tilde{\rho}}(\tilde{\rho}, s), \phi \right\rangle &= \int_{\Omega} \alpha \nabla \mathcal{P}_{\varepsilon}(\tilde{\rho}) \cdot \phi + \nu_1 \phi_1 + \nu_2 \phi_2 \, dx \\ &+ \sum_{j=1}^{n} \sum_{i=1}^{3} \int_{\Omega} a'(\rho_i) (\mathbb{C}_i \left(\mathrm{e}(u_j) - \beta_i s_j \mathrm{I}_d \right) \cdot \mathrm{e}(\lambda_j^*) \phi_i \, dx + \int_{\Omega} \nabla_{\tilde{\rho}} Q(\tilde{\rho}, \mathrm{s}) \cdot \phi \, dx, \quad (4.4.7) \end{aligned}$$

with the convention $\phi_1 = 1 - \phi_2 - \phi_3$.

Similarly, for $\psi \in [H^1(\Omega)]^2$, the directional derivative of J with respect to s in the direction ψ is given by:

$$\left\langle \frac{\partial J}{\partial \mathrm{s}}(\rho, \mathrm{s}), \psi \right\rangle \quad = \quad \left\langle \frac{\partial \mathcal{L}}{\partial u_1}, \frac{\partial u_1}{\partial \mathrm{s}}\psi \right\rangle \; + \; \cdots \; + \; \left\langle \frac{\partial \mathcal{L}}{\partial u_n}, \frac{\partial u_n}{\partial \mathrm{s}}\psi \right\rangle \; + \; \left\langle \frac{\partial \mathcal{L}}{\partial \mathrm{s}}, \psi \right\rangle \quad (4.4.8)$$

and with the same choice of Lagrange multipliers $\lambda_1^*, \ldots, \lambda_n^*$ satisfying the adjoint

equations (4.4.6), we get

$$\left\langle \frac{\partial J}{\partial \mathrm{s}}(\rho, s), \Psi \right\rangle = -\sum_{i=1}^{3} \int_{\Omega} \left[\mathbb{C}_i a(\rho_i) \left(\beta_i \mathrm{I}_2\right) \cdot \mathrm{e}(\lambda_j^*) \right] \cdot \psi_i \, dx + \nabla_{\mathrm{s}} Q(q, \mathrm{s}) \cdot \psi \, dx. \quad (4.4.9)$$

At each iteration of TAO's BNCG solver, given $(\tilde{\rho}, \mathrm{s})$, the computation of the sensitivity of our objective function with respect to a design change (resp. with respect to a stimulus change) involves computing the equilibrium displacements $u_1(\tilde{\rho}, \mathrm{s}), \ldots u_n(\tilde{\rho}, \mathrm{s})$ by solving n linearized elasticity problems (4.2.4), then computing the associated adjoint variables $\lambda_1^*, \ldots, \lambda_n^*$ using (4.4.6) before evaluating (4.4.7) (resp. (4.4.9).)

4.4.2 Minimization with respect to s

Observe that, minimizing the objective function (4.4.3) is equivalent to minimizing the Lagrangian (4.4.4) associated with the objective function. For simplicity, we only consider one prescribed displacement $\bar{u}$ and its corresponding stimulus s. For a fixed design ρ, the minimization with respect to s is equivalent to

$$\begin{cases} \min\limits_{s \in \mathcal{S}} \quad \mathcal{L}(u(\rho), \rho, s, \lambda) \text{ defined in (4.4.4)} \\ \\ \text{subject to} \quad -1 \leq s \leq 1. \end{cases} \quad (4.4.10)$$

By expanding the Lagrangian (4.4.4) and collect all the terms explicitly depending on s, we have

$$\begin{aligned}
\min_{s\in\mathcal{S}} \mathcal{L}(u(\rho),\rho,s,\lambda) &\iff \min_{s\in\mathcal{S}} -\int_\Omega s\rho_3^2\mathbb{C}_3\mathrm{I}_2\cdot \mathrm{e}(\lambda)\,dx + \int_\Omega ((1-\rho_2-\rho_3)^2+\rho_2^2)s^2\,dx,\\
&\iff \min_{s\in\mathcal{S}} -s\rho_3^2\mathbb{C}_3\mathrm{I}_2\cdot \mathrm{e}(\lambda) + ((1-\rho_2-\rho_3)^2+\rho_2^2)s^2\\
&\iff \min_{s\in\mathcal{S}} -s\rho_3^2\mathbb{C}_3\mathrm{e}(\lambda)\cdot \mathrm{I}_2 + ((1-\rho_2-\rho_3)^2+\rho_2^2)s^2\\
&\iff \min_{s\in\mathcal{S}} -s\rho_3^2 d\kappa_3 \mathrm{tr}(\mathrm{e}(\lambda)) + ((1-\rho_2-\rho_3)^2+\rho_2^2)s^2,
\end{aligned}$$

where $\kappa_3 = \frac{d\lambda_3^{**}+2\mu_3^{**}}{d}$ is the bulk modulus of the responsive material. The expression above is quadratic in s in the form of $As + Bs^2$ and its minimizer s^* is given as: if $A = 0$, then $s^* = 0$, and if $2B < |A|$ then $s^* = 1$ (resp. -1) if $\mathrm{tr}(\mathrm{e}(\lambda)) > 0$ (resp. $\mathrm{tr}(\mathrm{e}(\lambda)) < 0$). Otherwise $s^* = A/2B$.

Remark 3. *As $\varepsilon \to 0$, one can see, if $\rho_3 = 0$ at any point $x \in \Omega$* i.e *we have no responsive material at point x, then the optimal stimulus at point x becomes* 0. *And if $\rho_3 = 1$ any point $x \in \Omega$* i.e *we have responsive material at point x, then the optimal stimulus becomes either* 1 *or* -1 *depending on the sign of tr*$(\mathrm{e}(\lambda))$. *and the closed form of an optimal stimulus is given as:*

$$\begin{cases} 1 & \text{if } tr(\mathrm{e}(\lambda)) > 0 \text{ and } \rho_3 = 1 \\ 0 & \text{if } \rho_3 = 0, \\ -1 & \text{if } tr(\mathrm{e}(\lambda)) < 0 \text{ and } \rho_3 = 1. \end{cases} \tag{4.4.11}$$

4.4.3 Minimization algorithm

Our implementation uses Firedrake [51], an open source automated system for the solution of partial differential equations using the finite element method. The displacement, density, and stimulus fields are discretized using linear Lagrange simplicial finite elements over unstructured meshes. The minimization algorithm we used is a BNCG (Bounded Nonlinear Conjugate Gradient) solver implemented in the TAO (Toolkit for Advanced Optimization) optimization package, which is a part of PETSc (the Portable, Extensible Toolkit for Scientific Computation) library [18–20]. BNCG only requires first order derivatives of the objective function, which we compute in close form (*i.e.* optimize then discretize) using the standard adjoint technique [43].

We tested two different numerical approaches: In a *monolithic scheme*, we jointly minimize $\mathcal{O}$ with respect to ρ and s simultaneously using (4.4.7) and (4.4.9). In a *staggered scheme*, we use TAO to minimize $\mathcal{O}$ with respect to ρ only. Whenever computing $\frac{\partial J}{\partial \rho}$ using (4.4.7), we perform a full minimization of $\mathcal{O}$ with respect to s using (4.4.11) after computing the state and adjoint variables u_j and λ_j $(1 \leq j \leq n)$.

In each case, we leverage TAO's line search [64] and convergence criteria.

Algorithm 1 Monolithic scheme

Require: Initial guess of ρ and s.

1: Discretize using P_1 elements.

2: Define the weak form of state and adjoint PDEs.

3: Define the Objective function $\mathcal{O}$ and define the Lagrangian $\mathcal{L}$ (4.4.4).

4: **while** $\|\text{gradient}\| > tolerance$ **do**

5: Compute sensitivities with respect to ρ and s.

6: Set TAO solver to BNCG

7: One step minimization gradient with respect to ρ and s.

8: **end while**

Algorithm 2 Staggered scheme

Require: Initial guess of ρ and s.

1: Discretize using P_1 elements.

2: Define the weak form of state and adjoint PDEs.

3: Define the Objective function $\mathcal{O}$ and define the Lagrangian $\mathcal{L}$ (4.4.4).

4: **while** $\|\text{gradient}\| > tolerance$ **do**

5: Compute sensitivity with respect to ρ.

6: Set TAO solver to BNCG

7: Minimization with respect to s.

8: One step minimization gradient with respect to ρ

9: **end while**

4.5 Numerical results

We present a series of numerical simulations illustrating the strengths of our approach. In all that follows, we use

$$W(\rho) := \rho_1^2(1-\rho_1)^2 + \rho_2^2(1-\rho_2)^2 + \rho_3^2(1-\rho_3)^2 \tag{4.5.1}$$

as the multi-well potential in $\mathcal{P}_\varepsilon$ (4.2.2). Note that although this function admits 8 roots in $\mathbb{R}^3$, once restricted to the hyperplane $\rho_1 + \rho_2 + \rho_3 = 1$, it admits only three roots and is therefore admissible in (4.2.2). Technically, W would need to be renormalized in order to satisfy (4.2.3). Since the parameter α in (4.1.8) does not have a physical meaning, it is not necessary to do so. We use a simple quadratic material interpolation function $a(s) := s^2$.

In the "void" material, we set the stiffness parameter to $\eta = 10^{-6}$ and the Poisson ratio to $\nu = 0.3$ for all materials and we consider varying elastic moduli ratios E_3/E_2 where E_3 and E_2 are elastic modulus for responsive and non-responsive material respectively.

Cantilever beam

We start with the simplest case of least square problem with only one prescribed displacement $\bar{u}$, *i.e* $n = 1$ in (5.2.3). The design domain $\Omega = (0, L_x) \times (0, L_y)$ with $L_x = 1$ and $L_y = 1/3$. We prescribe null displacement on the left side Γ_D of Ω and set $\Omega_0 = (L_x - a, L_x) \times (L_y/2 - a/2, L_y/2 + a/2)$ with $a = 1/15$.

The prescribed displacement on Ω_0 is taken as $\bar{u} = [0, 1]^T$ *i.e.* we want the region Ω_0 to move upward. The domain Ω is discretized with a structured mesh with cell

size $h = 2 \times 10^{-3}$. The regularization parameter is $\varepsilon = 2 \times 10^{-3}$ and the perimeter penalization parameter is $\alpha = 6 \times 10^{-4}$. The relative and absolute tolerance on the gradient and objective function in TAO were set to 1×10^{-6} as it was observed that tighter tolerances do not lead to significant differences in the designs produced.

We first compare the numerical approaches described above. Figure 4.1 shows the density of non-responsive (ρ_2) and responsive (ρ_3) materials, as well as a composite plot showing the non-responsive material in black and the responsive material coloured according to the value of the stimulus s_1 with $s_1 = -1$ in red, $s_1 = 0$ in white, and $s_1 = 1$ in blue. In both case, ρ_2 and ρ_3 are initialized with a constant value 0.3. The penalty terms are set to $\nu_2 = 0.1$ and $\nu_3 = 0.3$, and both materials are isotropic homogeneous with non-dimensional Young's modulus 5 and Poisson ratio 1.

We observe that both methods lead to different but well-defined designs, exempt of checkerboards, were the material densities are well focussed near 0 and 1, as expected in the phase-field approach. The monolithic approach converged in 380 iterations of TAO's BNCG solver. The final value of the objective function is $\mathcal{O} = 4.49 \times 10^{-1}$. The staggered solver converged in just 173 iteration leading to an objective function $\mathcal{O} = 4.17 \times 10^{-3}$.

Based on this result, all results presented further in this article were computed using the staggered scheme.

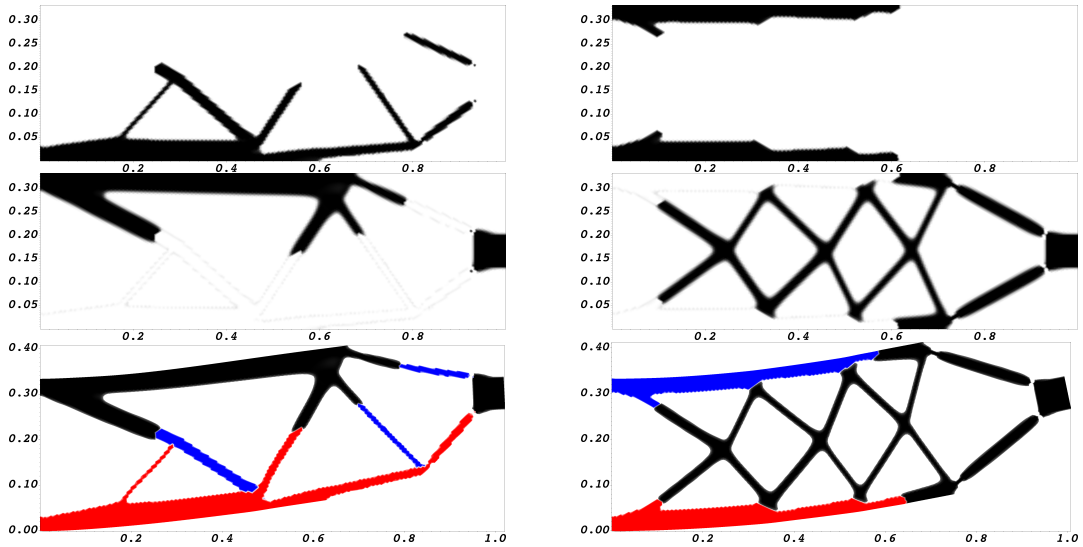

Figure 4.1: Monolithic (left) vs. staggered (right) scheme. Responsive material density (top), non-responsive material density (middle), and composite plot of both material density and the stimulus in the deformed configuration.

Changing the ratio of the Young's modulus of the two materials leads to very different designs. In Figure 4.2, the Young's modulus of the non-responsive material has been increased to 10. The penalty terms are respectively $\nu_2 = 0.24$ and $\nu_3 = 0.12$ (left) and $\nu_2 = 0.18$ and $\nu_3 = 0.12$ (right). When the penalty term on the stiffer, non-responsive material is high enough, the structure consists entirely of the weaker responsive material, whereas decreasing this parameter leads back to rigid truss-like structures activated by small regions of responsive material.

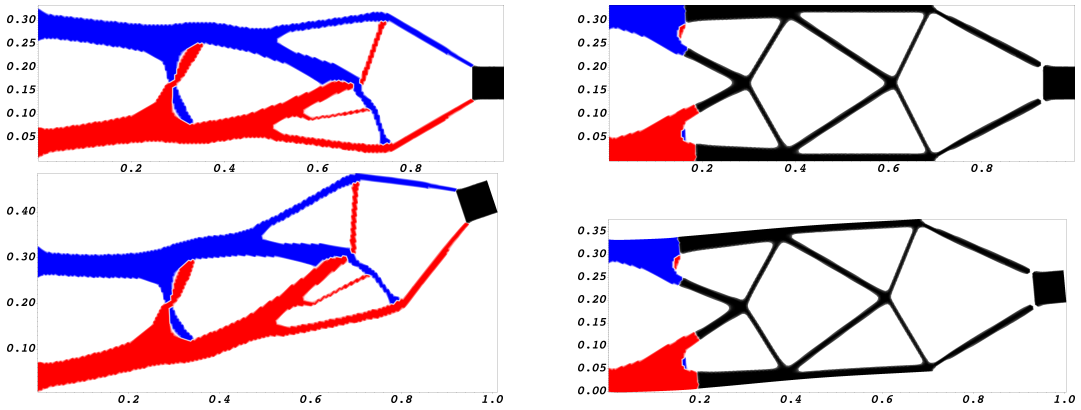

Figure 4.2: Optimized structure with a ratio $E_2/E_3 = 2$ in the reference (top) and deformed configuration (bottom) with $\nu_3 = 0.12$ and $\nu_2 = 0.24$ (left) and $\nu_2 = 0.18$ (right).

4.5.1 Cantilever beam with two target displacements

In a second numerical example, we consider two target displacements ($n = 2$ in (5.2.3)). The young's modulus of both materials is set to 5. In Figure 4.3, the target displacements are $(0, 1)$ and $(0, 2)$. The penalty terms are $\nu_2 = 0.5$ and $\nu_3 = 0.7$, leading to volume fraction of the responsive and non-responsive material of respectively 15% and 21%. As the materials are linear elastic, approaching the target displacement $(0, 1)$ could have been obtained by rescaling the stimulus in of target displacement $(0, 2)$. Instead, our scheme generates a more complex geometry and activation scheme.

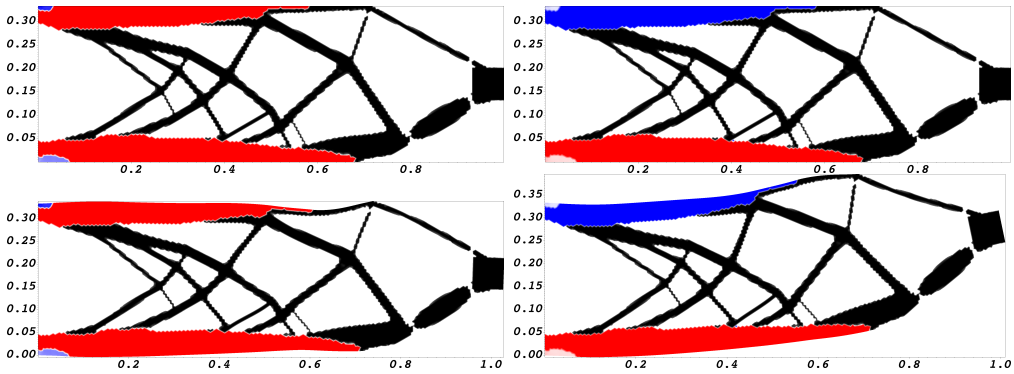

Figure 4.3: Optimal design of a beam with two target displacements. (left) Material distribution and stimulus for a target displacement of $(0, 1)$ in the reference (top) and deformed (bottom) configuration. (right) Material distribution and stimulus for a target displacement of $(0, 2)$ in the reference (top) and deformed (bottom) configuration.

In Figure 4.4, the target displacements are $(1, 0)$ and $(0, 1)$. All other parameters remain the same as in Figure 4.3. The volume fraction of responsive and non-responsive material are respectively 12% and 9%. The responsive material is laid out in simple regions while the non-responsive material layout forms a stiff truss structure.

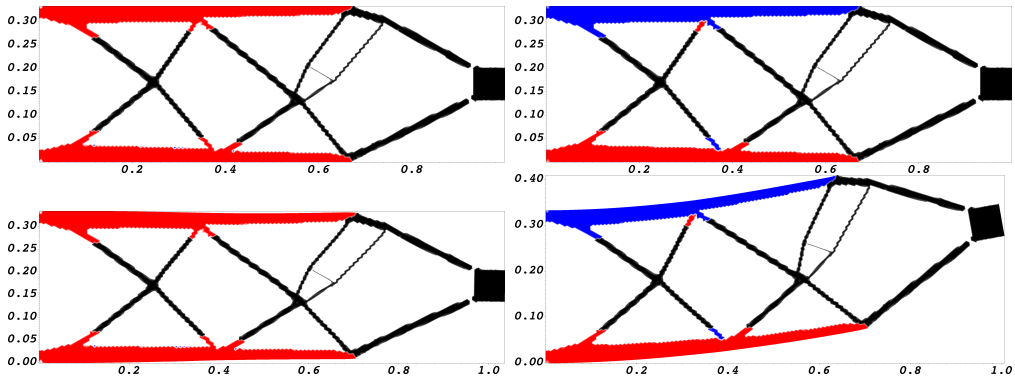

Figure 4.4: Optimal design of a beam with two target displacements. (left) Material distribution and stimulus for a target displacement of $(1, 0)$ in the reference (top) and deformed (bottom) configuration. (right) Material distribution and stimulus for a target displacement of $(0, 1)$ in the reference (top) and deformed (bottom) configuration.

4.5.2 Hexagonal domain with three target displacements

Our third example is inspired by the Stewart platform parallel manipulator. We consider a regular hexagonal domain with edge length 0.35 clamped on three non-consecutive edges (see Figure 4.5). The target displacements of a centered regular hexagon with edge length 0.035 are $\bar{u}_1 = (\cos(0), \sin(0))$, $\bar{u}_2 = (-\cos(\pi/3), \sin(\pi/3))$ and $\bar{u}_3 = (-\cos(\pi/3), -\sin(\pi/3))$.

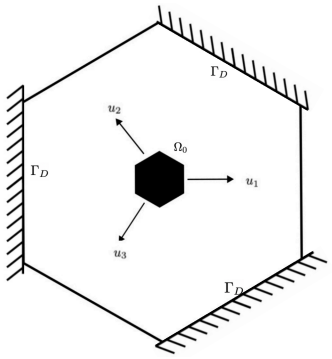

Figure 4.5: Hexagonal domain clamped at three sides Γ_D

In Figure 4.6, the Young's modulus of the responsive and non-responsive materials are set to 5×10^{-3} and 5×10^{-2} respectively. The penalty factor on the stiffer material is set to a much higher value than that of the responsive materials ($\nu_2 = 0.7$ and $\nu_3 = 0.03$). The perimeter penalty factor is set to 3.5×10^{-4} and the regularization length to 2×10^{-3}, as above. This leads to slender structures activated by large "pads". We note that although that designs and stimuli are invariant by a $2\pi/3$ rotational symmetry, which was not enforces in the computations.

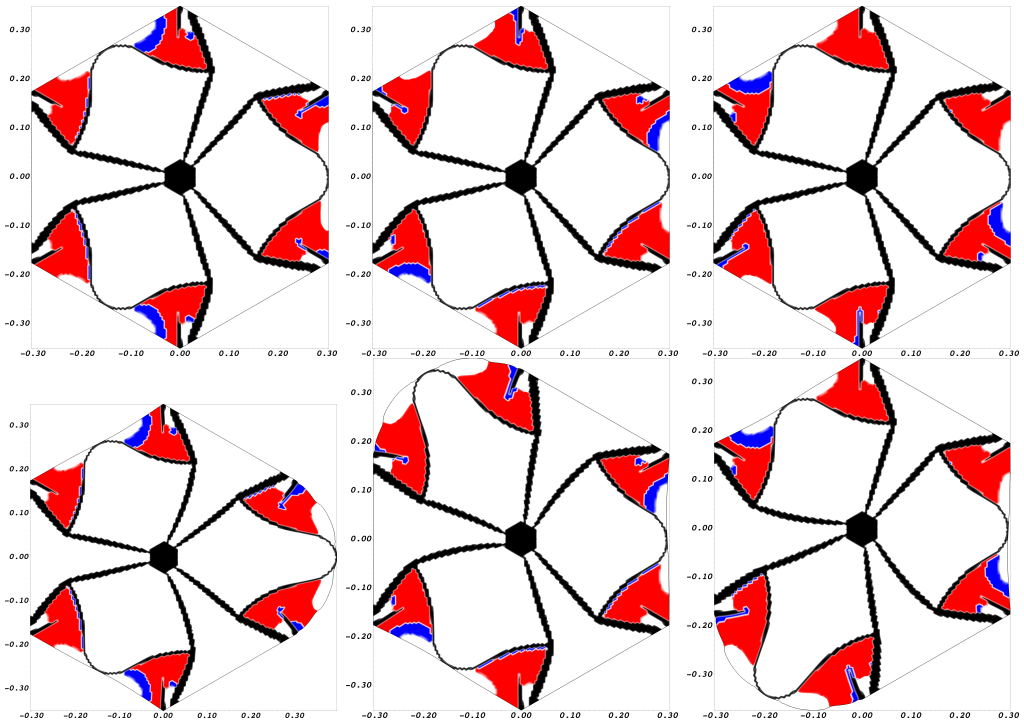

Figure 4.6: Optimal design with three prescribed displacement with $E_2/E_3 = 10$ and a strong penalty on the stiff material.

When reducing the elastic contrast between materials ($E_2 = 5 \times 10^{-2}$ and $E_3 = 1 \times 10^{-2}$) and slightly decreasing the cost of the stiff material ($\nu_2 = 0.3$ and $\nu_3 = 0.03$), we obtain a simpler geometry with larger areas occupied by responsive material. Again, deformation towards the target displacement is achieved by flexing elongated stiff structures (see Figure 4.7).

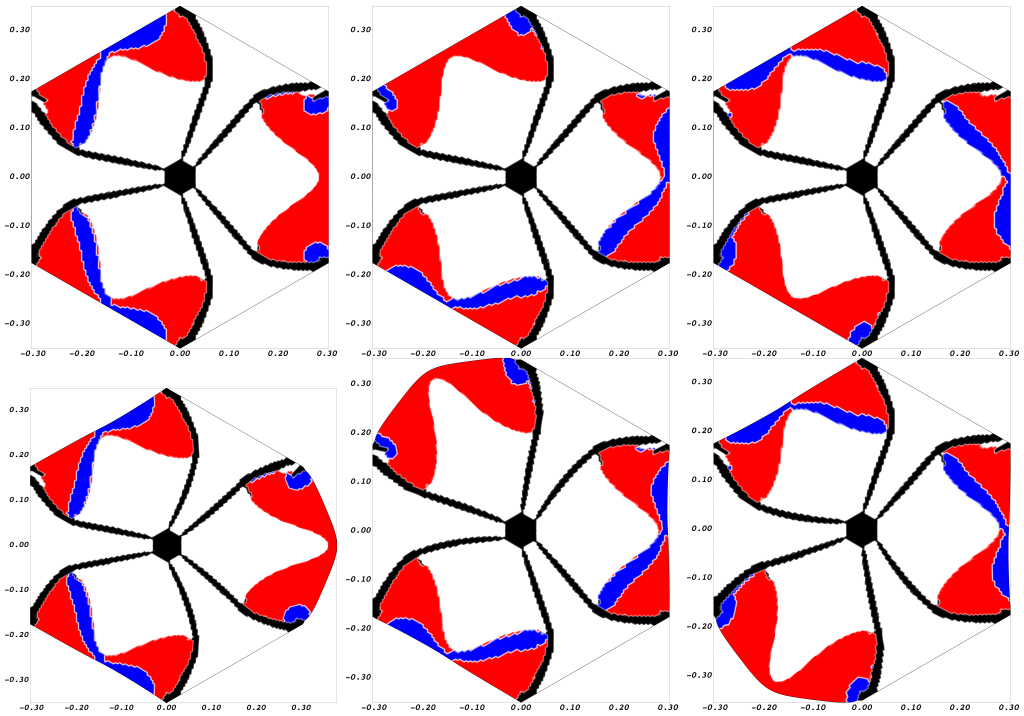

Figure 4.7: Optimal design with three prescribed displacement with $E_2/E_3 = 5$ and a strong penalty on the stiff material.

Finally, when using a stiff responsive material and weaker non-responsive materials ($E_2 = 1 \times 10^{-2}$ and $E_3 = 5 \times 10^{-2}$), all other parameters remaining the same, we obtain designs consisting solely of the responsive materials. This is expected since in this situation, the non-responsive material is both expensive, less stiff, and incapable of activation.

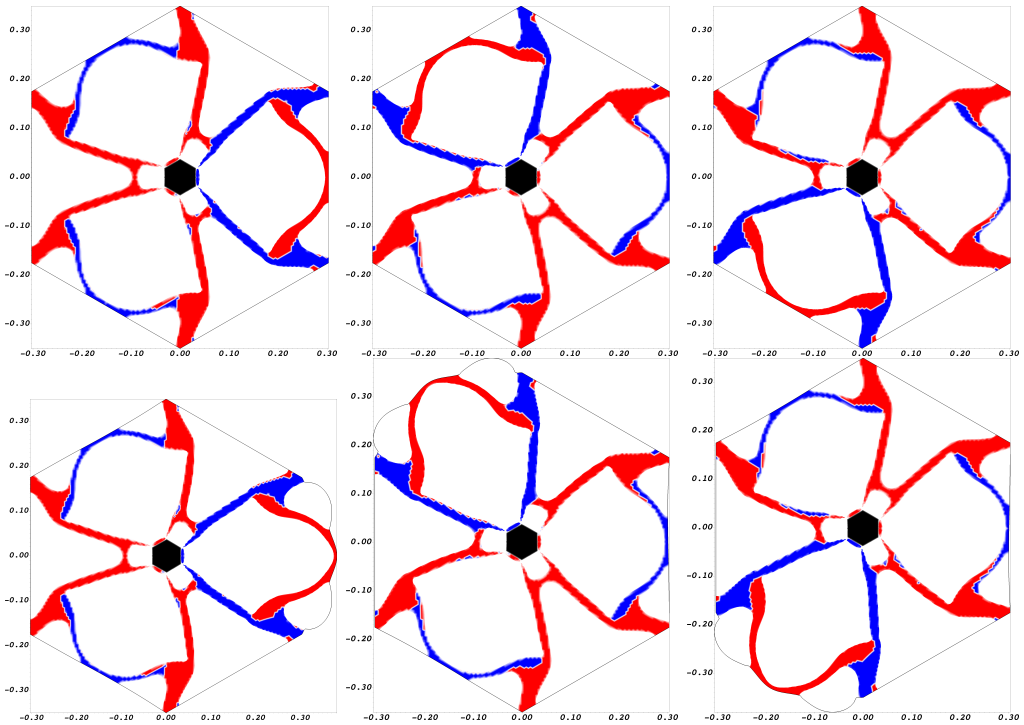

Figure 4.8: Optimal design with three prescribed displacement with $E_2/E_3 = 0.2$ and a strong penalty on the stiff material.

4.6 Conclusion

We have investigated the systematic design of responsive structures with a prescribed target displacement and perimeter constraint. We proved existence of solutions to a phase-field regularization phase-field problem and their convergence to that of the "sharp interface" problem. We proposed a numerical scheme based on an iterative gradient-based solver with respect to one set of design variable (the materials' density) where at each step a full minimization of the objective function with respect to the second set of design variables (the stimuli) is performed. Our approach is illustrated

by series of numerical examples demonstrating its ability to identify complex geometries and produced well-delineated "black and white" design, owing to the well-pose natures of the phase-field regularization.

While this work focused on a simple actuation mechanism in the form of an isotropic inelastic strain, accounting for to more complex stimuli and responsive materials including piezo-electrics, dielectric elastomers and liquid crystal elastomers or shape memory alloys should be a relatively simple extension of this work. Whereas the objective function used here focus solely on kinematics of a structure, the framework could be extended to optimization of mechanical advantage as in [2, 73].

A natural extension of the work presented in this article is to consider a stimulus derived from a physical process. In this setting, the stimulus itself would become a state variable, derived from solving a PDE governed by some additional design variable. For instance, one could consider body or boundary heat flux as design variables, and the temperature field as a state variable.

Chapter 5

Systematic design of compliant morphing structures with stimulus as state variable

5.1 Introduction

We extend the responsive optimal design problem by considering the stimulus as a state variable computed by solving a PDE governed by some additional design variable. For instance, one could consider body or boundary heat flux as design variables, and the temperature field as a state variable.

In all that follows, we focus on the spacial case of three isotropic linear elastic materials, "void", a non-responsive material, and a responsive material with density ρ_1, ρ_2 and ρ_3 respectively.

5.2 Stimulus governed by poisson PDE

We start with by extending problem (4.2.5) by considering a stimulus s computed by solving the Poisson PDE characterized by a design variable, the stimulus control function g. Consider an inelastic strain

$$\sigma = \sum_{i=1}^{3} \mathbb{C}_i \left(\mathrm{e}(u) - \beta_i s \mathrm{I}_d \right) \tag{5.2.1}$$

where where $\mathbb{C}_i$ denotes the Hooke's law for material i, $\mathrm{e}(u)$ is the linearized strain associated to a displacement field u, I_d the $d \times d$ identity matrix and $\beta \geq 0$ is a given parameter such $\beta_1 = \beta_2 = 0$ in (5.2.1). In the responsive material, we set $\beta_3 = 1$. Here we consider stimulus of the form $s\mathrm{I}_d$ such that when the responsive material is heated, *i.e* $s > 0$ (resp. cooled *i.e* $s < 0$) and the responsive material expands (resp. contracts) horizontally. The stimulus $s \in V$ is governed by Poisson's equation

$$-\nabla \cdot (k(\mathrm{D}) \nabla s) = g \text{ in } \Omega, \ \nabla s \cdot \vec{n} = 0 \text{ on } \Gamma_N, s = 0 \text{ on } \Gamma_D \tag{5.2.2}$$

where $k(\mathrm{D})$ is simple material interpolation. We then seek to minimize

$$\mathcal{I}(u) := \frac{1}{2} \int_{\Omega_0} |u - \bar{u}|^2 \, dx, \tag{5.2.3}$$

amongst a set $\mathcal{D}$ of admissible designs and a space of stimulus control functions $\mathcal{G}$ *i.e.*

$$\mathcal{G} := \left\{ g \in L^\infty(\Omega); \ ||g||_\infty \leq 1 \right\}. \tag{5.2.4}$$

5.3 Numerical implementation

Due to the ill-posedness of (5.2.3), we once again employ the phase-field approach to optimal design [28, 29] discussed in section (4.2). We introduce generalized designs of the form

$$\rho = (\rho_1, \rho_2, \rho_3) \in \left[H^1(\Omega; [0,1])\right]^3, \tag{5.3.1}$$

where the $\rho_i, i = 1, 2, 3$ are smooth continuous material densities with values in $[0, 1]$ such that $\rho_1 + \rho_2 + \rho_3 = 1$ for all $x \in \Omega$. We handle the constraint $\rho_1 + \rho_2 + \rho_3 = 1$ explicitly by substituting $\rho_1 = 1 - \rho_2 - \rho_3$ and optimizing with respect to $\tilde{\rho} = (\rho_2, \rho_3)$ under the constraint $0 \leq \rho_2, \rho_3 \leq 1$. To this end, we define the regularization of (5.2.3) as:

$$\begin{cases} \min\limits_{(\rho,g)} \dfrac{1}{2} \displaystyle\int_{\Omega_0} |u - \bar{u}|^2 dx + \alpha \mathcal{P}_\varepsilon(\tilde{\rho}) \\ \\ \text{subject to (4.2.4) and (5.2.2)} \end{cases} \tag{5.3.2}$$

where α is an arbitrary regularization parameter.

Since we have two PDE constraints, we need two adjoint variables and we define the Lagrangian accordingily,

$$\begin{aligned} \mathcal{L}(u, \rho, \lambda, g, s, q) = \frac{1}{2} \int_{\Omega_0} |u - \overline{u}|^2 \, dx \; + \; \alpha \mathcal{P}_\varepsilon(\tilde{\rho}) + Q(\tilde{\rho}, g) \\ + \sum_{i=1}^{3} \int_\Omega a(\rho_i) \mathbb{C}_i \left(\mathrm{e}(u) - \beta_i s \mathrm{I}_d\right) \cdot \mathrm{e}(\lambda) \, dx \\ + \sum_{i=1}^{3} \int_\Omega k(\rho_i) \nabla s \cdot \nabla q \, dx - \int_\Omega g \, q \, dx \end{aligned} \tag{5.3.3}$$

where λ and q are the adjoint variables associated with displacement field u and the

stimulus s respectively. The penalty $Q(\tilde{\rho}, g)$ is defined as

$$Q(\tilde{\rho}, g) = \int_\Omega ((1-\rho_2-\rho_3)^2 + \rho_2^2) g^2 \, dx \tag{5.3.4}$$

to enforce null-heat source $i.e\ g = 0$ in "void" and non-responsive materials. Applying the adjoint method, one obtains the following adjoint weak formulations to be solved before computing the sensitivities with respect to ρ and g

$$\sum_{i=1}^{3} \int_\Omega a(\rho_i) \mathbb{C}_i \mathrm{e}(v) \cdot \mathrm{e}(\lambda) \, dx = \int_{\Omega_0} (u - \overline{u}) v \, dx, \text{ for any } v \in V \tag{5.3.5}$$

$$\sum_{i=1}^{3} \int_\Omega k(\rho_i) \nabla w \cdot \nabla q \, dx = \sum_{i=1}^{3} \int_\Omega a(\rho_i) \mathbb{C}_i \beta_i w \mathrm{I}_d \cdot \mathrm{e}(\lambda) \, dx, \text{ for any } w \in V. \tag{5.3.6}$$

5.3.1 Minimization with respect to g

Observe that, by expanding the Lagrangian (5.3.3) and collect all the terms explicitly depending on g, we have

$$\begin{aligned} \min_{g \in \mathcal{G}} \mathcal{L}(u, \rho, g, \lambda, s, q) &\iff \min_{g \in \mathcal{G}} - \int_\Omega gq \, dx + \int_\Omega ((1-\rho_2-\rho_3)^2 + \rho_2^2) g^2 \, dx, \\ &\iff \min_{g \in \mathcal{G}} -gq + ((1-\rho_2-\rho_3)^2 + \rho_2^2) g^2. \end{aligned}$$

The expression above is quadratic in g in the form of $Ag + Bg^2$ and its minimizer g^* is given as: if $A = 0$, then $g^* = 0$, and if $2B < |A|$ then $g^* = 1$ (resp. -1) if $q > 0$ (resp. $q < 0$). Otherwise $g^* = A/2B$.

5.4 Numerical results

In this section, we present a series of numerical simulations and in all of our results, consider the design domain $\Omega = (0, L_x) \times (0, L_y)$ with $L_x = 1$ and $L_y = 1/3$. We prescribe null displacement on the left side Γ_D of Ω and set $\Omega_0 = (L_x - a, L_x) \times (L_y/2 - a/2, L_y/2 + a/2)$ with $a = 1/15$. We use the same multi-well potential W defined in (4.5.1). The responsive and non-responsive materials are isotropic with varying stiffness ratios E_3/E_2 and Young's modulus for void is fixed $E_1 = 10^{-6}$ and Poison ratio $\nu = 0.3$. The domain Ω is discretized with a structured mesh with cell size $h = 0.002$. The regularization parameter is $\varepsilon = 2.0 \times 10^{-3}$ the perimeter penalization parameter is $\alpha = 6.0 \times 10^{-3}$. The initial design fields are chosen as $\rho_3 = 0.3, \rho_2 = 0.3$ and $\rho_2 = 1$ in Ω_0.

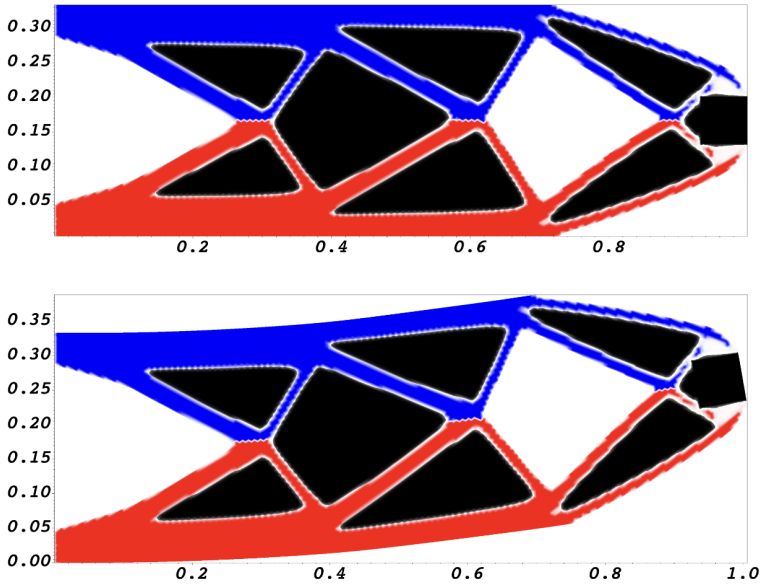

Figure 5.1: Composite plot of both material density and the heat source in the reference (top) and deformed configuration (bottom) for stiffness ratio $E_3/E_2 = 100$. The red and blue represent the area of the responsive material with heat source values 1 and -1 respectively. The converged design consists of 33% responsive and 34% non-responsive material.

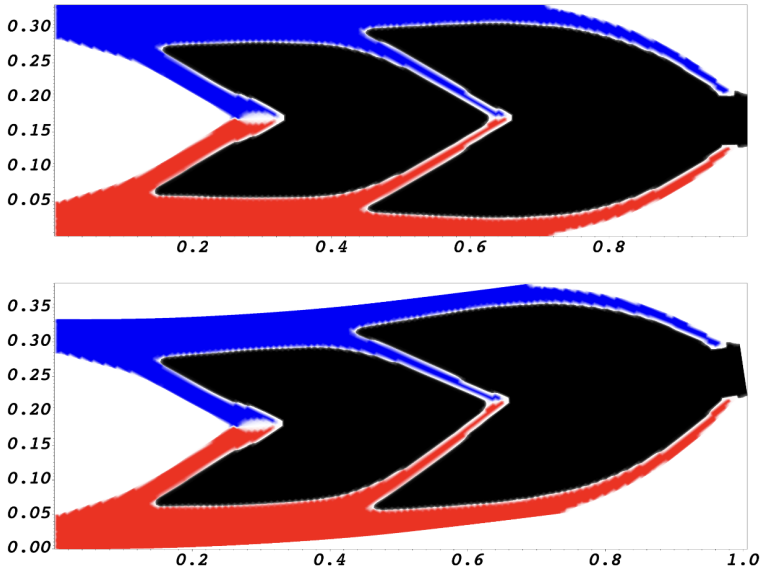

Figure 5.2: Composite plot of both material density and the heat source in the reference (top) and deformed configuration (bottom) for stiffness ratio $E_3/E_2 = 10$. The red and blue represent the area of the responsive material with heat source values 1 and -1 respectively. The converged design consists of 30% responsive and 50% non-responsive material.

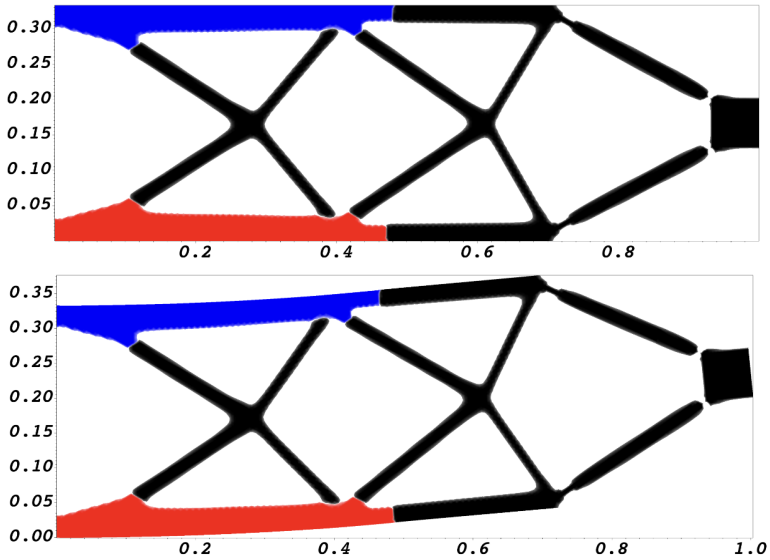

Figure 5.3: Composite plot of both material density and the heat source in the reference (top) and deformed configuration (bottom) for stiffness ratio $E_3/E_2 = 1$. The red and blue represent the area of the responsive material with heat source values 1 and -1 respectively. The converged design consists of 12% responsive and 18% non-responsive material

In our first results, Figure (5.1) and (5.2), we consider the responsive material to be 100 and 10 stiffer than the non-responsive material. As expected, final design uses the stiffer material to build the outer frame of the beam. The distribution of the stimulus makes the converged design to act as "bimetallic" strip in sense that, when stimulated the responsive material at the top contracts horizontally while the responsive material at the bottom expands horizontally, causing the beam to do work against the applied load as shown in the last figure in Figure (5.2) above.

In the next Figure (5.3), we consider the responsive material to have the same stiffness as the non-responsive material. As expected, the converged design did not change very much from the that in Figure (5.2) above in a sense that the stronger

material is used to build the frame. In this computation, our algorithm converged after 843 iterations leading to the objective function to decrease from 8.4521 to 0.1938.

Our next example, we consider a case where the stimulus control function g can only takes values in $[0, 1]$. Figure (5.4) shows the density of non-responsive (ρ_2) and responsive (ρ_3) materials, as well as a composite plot showing the non-responsive material in black and the responsive material coloured according to the value of the heat source g with $g = 1$ in red, $g = 0$ in gray, and the white region represents the "void". As one would expect, the converged design did not change much, only the heat source is turned on at the bottom and off at the top so that the design expands at the bottom and pushing Ω_0 upward as shown in Figure (5.4).

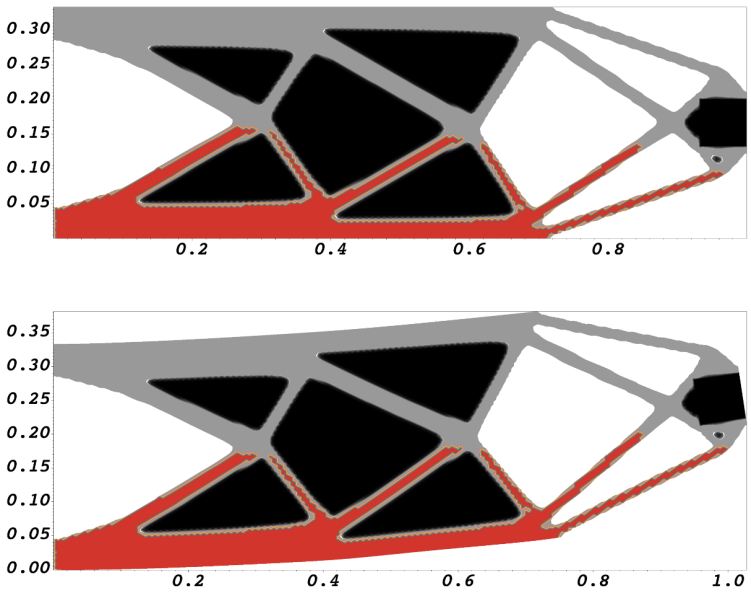

Figure 5.4: Composite plot of both material density and the heat source in the reference (top) and deformed configuration (bottom) for stiffness ratio $E_3/E_2 = 100$. The red and gray represent the area of the responsive material with heat source values 1 and 0 respectively. The converged design consists of 34% responsive and 29% non-responsive material.

5.5 Stimulus governed by transient heat PDE

We extend problem (4.2.5) further by introducing time-dependent objective function of the form

$$\min_{(\rho,\, g)} \frac{1}{2} \int_0^T \int_{\Omega_0} |u(t,x) - \overline{u}(t,x)|^2 \, dx \tag{5.5.1}$$

where $u(t,x)$ is the solution of the linearized PDE (4.2.4) dependent on time-dependent stimulus $s(t,x)$ at each time step and $\overline{u}(t,x)$ is a given path we want the region Ω_0 to

follow. The time-dependent stimulus $s(t,x)$ is controlled by a transient heat equations

$$\begin{cases} s_t = \nabla \cdot (k(\mathrm{D})\nabla s) + g \text{ in } \Omega \times (0,T), \\ s(0,x) = 0 \quad \text{ in } \ \Omega \times (0,T), \\ s(t,x) = 0 \text{ on } \Gamma_D \times (0,T), \\ \nabla s \cdot n = 0 \quad \text{ on } \ \Gamma_N \times (0,T), \end{cases} \tag{5.5.2}$$

where g is the heat source which depends on both time and space.

The sensitivity analysis with respect to ρ is similar to previous problems. For sensitivity analysis with respect to g, we define the Lagrangian as

$$\begin{aligned} &\mathcal{L}(u,\rho,\lambda,g,s,q) = \\ &\quad \frac{1}{2}\int_0^T \int_{\Omega_0} |u(t,x) - \overline{u}(t,x)|^2 \, dxdt \ + \ \alpha \mathcal{P}_\varepsilon(\rho) \\ &\quad + \sum_{i=1}^{3} \int_\Omega a(\rho_i)\mathbb{C}_i \left(\mathrm{e}(u) - \beta_i s \mathrm{I}_d\right) \cdot \mathrm{e}(\lambda) \, dx \\ &\quad + \int_0^T \int_\Omega s_t q \, dxdt - \int_0^T \sum_{i=1}^{3} \int_\Omega k(\rho_i)\nabla s \cdot \nabla q \, dxdt \\ &\quad - \int_0^T \int_\Omega g \cdot q \, dxdt. \end{aligned} \tag{5.5.3}$$

where λ and q are time-dependent adjoint variables. Following the steps of the adjoint method, we get the weak form of adjoint PDE for s

$$\int_0^T \sum_{i=1}^{3} \int_\Omega a(\rho_i)\mathbb{C}_i\beta_i w \mathrm{I}_d \cdot \mathrm{e}(\lambda) \, dxdt - \int_0^T \int_\Omega w_t q \, dxdt + \int_0^T \sum_{i=1}^{3} \int_\Omega k(\rho_i)\nabla w \cdot \nabla q \, dxdt = 0$$

for some test function w. Performing integration by parts in time and space

$$\begin{aligned}
&\int_0^T \sum_{i=1}^{3} \int_\Omega a(\rho_i)\mathbb{C}_i\beta_i w \mathrm{I}_d \cdot \mathrm{e}(\lambda)\, dxdt + \int_0^T \int_\Omega w q_t\, dxdt \\
&- \int_\Omega q(T,x)w(T,x)dx - \int_0^T \sum_{i=1}^{3} \int_\Omega k(\rho_i)\nabla\cdot\nabla q w dxdt \\
&+ \int_0^T \sum_{i=1}^{3} \int_\Omega k(\rho_i)(\nabla q \cdot n) w dxdt = 0.
\end{aligned} \tag{5.5.4}$$

Equation (5.5.4) can be written in strong form as

$$\begin{cases}
\quad q_t = \nabla\cdot(k(\mathrm{D})\nabla q) - a(\mathrm{D})\mathbb{C}\beta \mathrm{I}_d \cdot \mathrm{e}(\lambda) \quad \text{in } \Omega\times(0,T) \\
q(T,x) = 0 \quad \text{in } \Omega\times(0,T), \\
\nabla q\cdot n = 0 \quad \text{on } \Gamma_N\times(0,T).
\end{cases}$$

5.6 Numerical implementation

A straightforward approach to solving time-dependent PDEs by the finite element method is to first discretize the time derivative by a finite difference approximation, which yields a sequence of stationary problems, and then turn each stationary problem into a variational formulation.

Let superscript n denote a quantity at time t_n, where n is an integer counting time steps. For example, s_n means s at time step n. A finite difference discretization in time first consists of sampling the PDE at some time step, say t_{n+1}:

$$\left(\frac{\partial s}{\partial t}\right)^{n+1} = \nabla\cdot(k(\mathrm{D})\nabla s^{n+1}) + g^{n+1} \tag{5.6.1}$$

The time-derivative can be approximated by a difference quotient. For simplicity and stability reasons, we choose a simple backward difference:

$$\left(\frac{\partial s}{\partial t}\right)^{n+1} \approx \frac{s^{n+1} - s^n}{\Delta t} \tag{5.6.2}$$

where Δt is the time discretization parameter. Combining (5.6.1) and (5.6.2) yields

$$\frac{s^{n+1} - s^n}{\Delta t} = \nabla \cdot (k(\mathrm{D})\nabla s^{n+1}) + g^{n+1}. \tag{5.6.3}$$

This is our time-discrete version of the transient heat equations (5.5.2), a so-called *backward Euler* or *implicit Euler* discretization.

We may reorder (5.6.3) so that the left-hand side contains the terms with the unknown s^{n+1} and the right-hand side contains computed terms only. The result is a sequence of spatial (stationary) problems for s^{n+1}, assuming s^n is known from the previous time step:

$$s^{n+1} - \Delta t \nabla \cdot (k(\mathrm{D})\nabla s^{n+1}) = s^n + \Delta t g^{n+1}, n = 0, 1, 2, \ldots, \tag{5.6.4}$$

$$s^0 = s_0 \tag{5.6.5}$$

Given s_0, we can solve for s^0, s^1, s^2 and so on.

We use a finite element method to solve (5.6.4), this requires turning the equations into weak forms. As usual, we multiply by a test function $w \in V$ and integrate second-derivatives by parts. Introducing the symbol s for the unknown s^{n+1}, the resulting weak form arising from formulation (5.6.4) can be conveniently written in

the standard notation:

$$a(s,w) = L(w) \text{ for any } w \in V$$

where

$$a(s,w) = \int_\Omega (sw + \Delta t k(\mathrm{D})\nabla s \cdot \nabla w) dx \tag{5.6.6}$$

$$L(w) = \int_\Omega (s^n + \Delta t g^{n+1}) w \, dx. \tag{5.6.7}$$

5.7 Numerical results

Using the same ground domain Ω, we consider the target displacement $\overline{u}(t,x)$ defined as:

$$\overline{u}(t,x) = \begin{cases} (0, 4t) & 0 \le t < 0.25, \\ (0, 2-4t) & 0.25 \le t < 0.75, \\ (0, 4t-4) & 0.75 \le t \le 1. \end{cases}$$

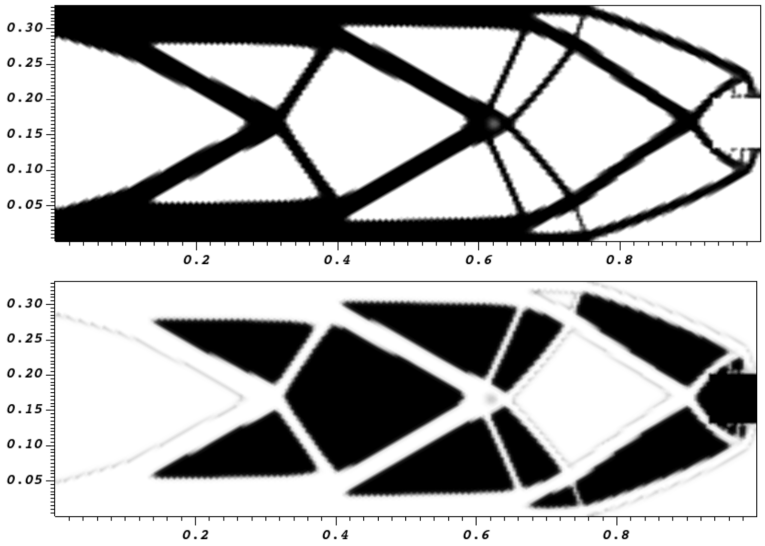

Figure 5.5: Responsive material density (top), non-responsive density (bottom) for stiffness ratio $E_3/E_2 = 100$.

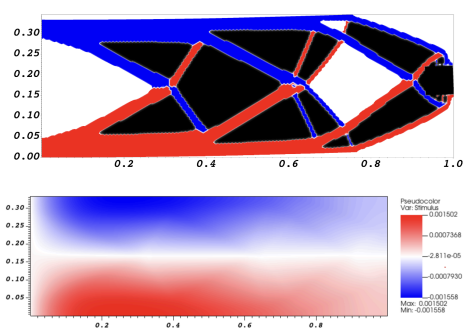

$t = 0.1$

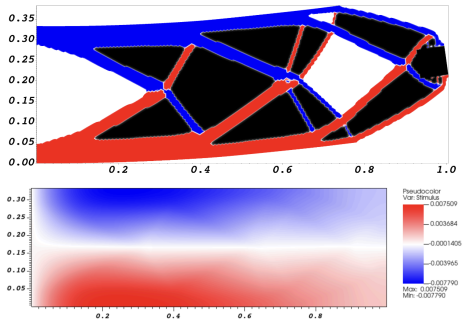

$t = 0.25$

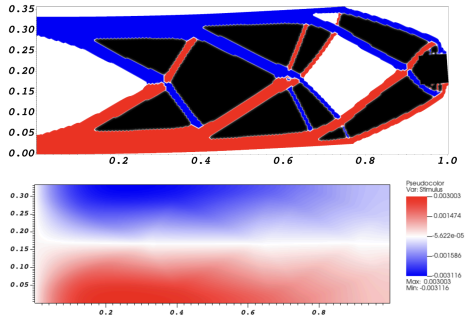

$t = 0.35$

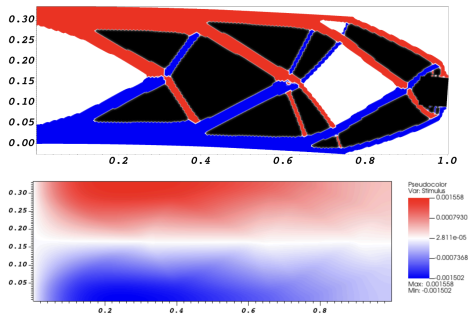

$t = 0.60$

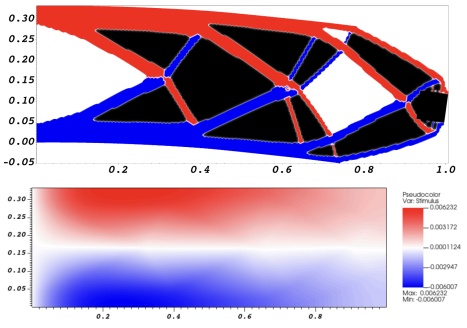

$t = 0.75$

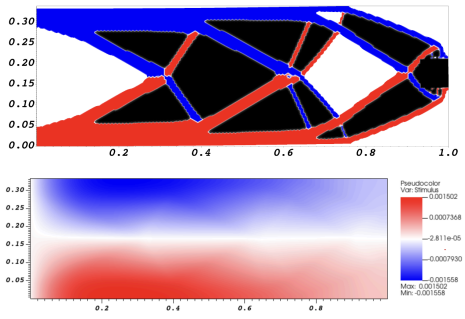

$t = 0.95$

Figure 5.6: Composite plot of both material density and the heat source in the deformed configuration (top row) and computed stimulus (bottom row) for stiffness ratio $E_3/E_2 = 100$ at different time steps. The red and blue (top row) represent the area of the responsive material with heat source values 1 and -1 respectively while the red and blue (bottom row) represent the areas where stimulus is positive and negative respectively.

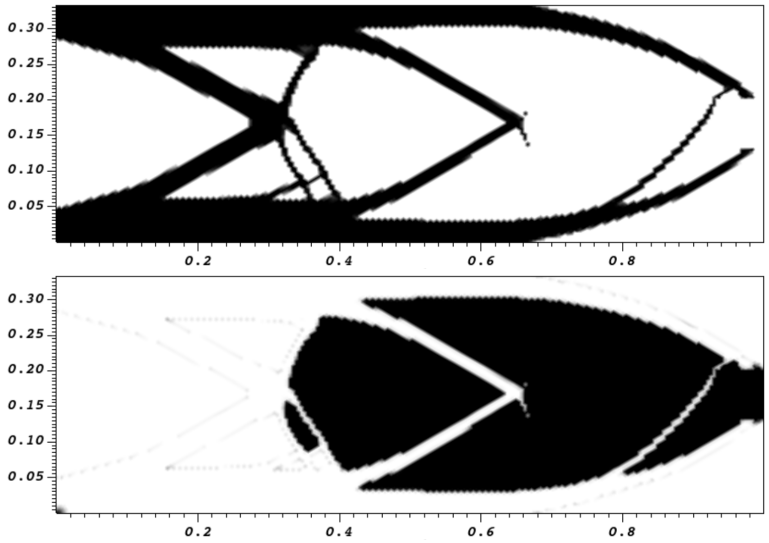

Figure 5.7: Responsive material density (top), non-responsive density (bottom) for stiffness ratio $E_3/E_2 = 10$.

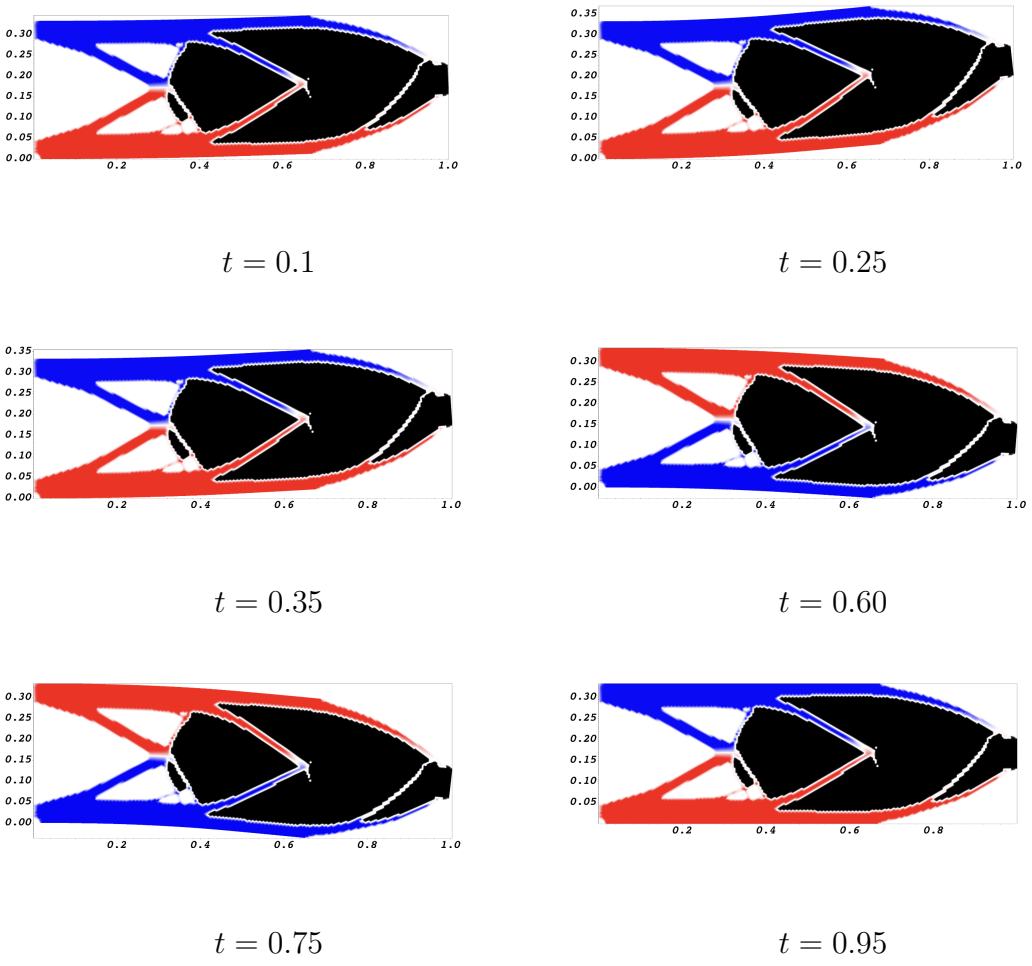

Figure 5.8: Composite plot of both material density and the heat source in the deformed configuration (top row) and computed stimulus (bottom row) for stiffness ratio $E_3/E_2 = 10$ at different time steps. The red and blue (top row) represent the area of the responsive material with heat source values 1 and -1 respectively.

In our first result, Figures (5.7) and (5.6) we consider the responsive material to be 100 and 10 stiffer than the non-responsive material. Our algorithm converged after 655 (resp. 977) iterations leading to the objective function to decrease from

13.8131(resp. 10.8172) to 0.8193(resp. 0.4512) for ratio 100(resp.10). As expected, final design uses the stiffer material to build the outer frame of the beam. The distribution of the stimulus makes the converged design to act as "bimetallic" strip in sense that, when stimulated the responsive material at the top contracts horizontally while the responsive material at the bottom expands horizontally, causing the beam to do work against the applied load as shown in the last figure in Figures (5.7) and (5.5) above.

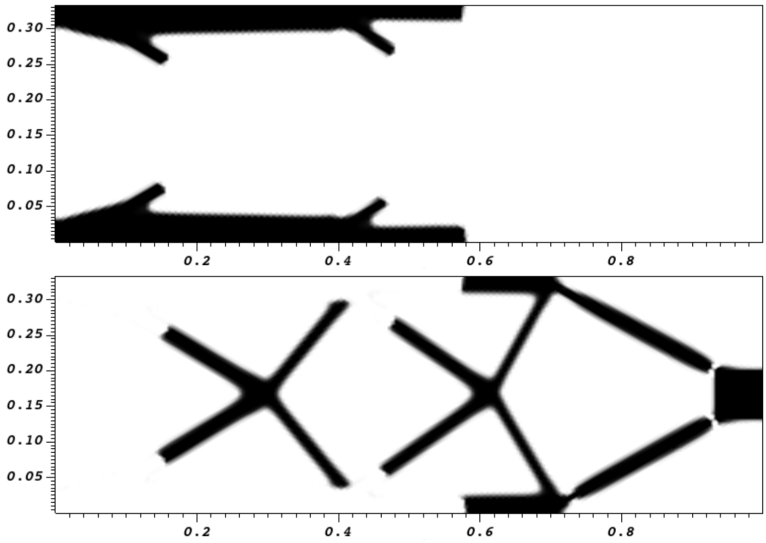

Figure 5.9: Responsive material density (top), non-responsive density (bottom) for stiffness ratio $E_3/E_2 = 1$.

In the next Figure (5.9), we consider the responsive material to be 1 stiffer than the non-responsive material. As expected, the converged design did not change very much from the that in Figure (5.9) above in a sense that the stronger material is used to build the frame. In this computation, our algorithm converged after 932 iterations

leading to the objective function to decrease from 8.7142 to 0.2509.

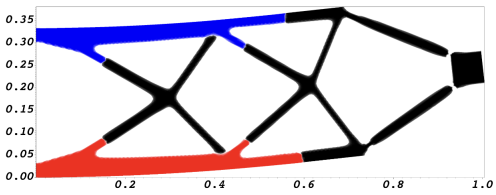

$t = 0.1$

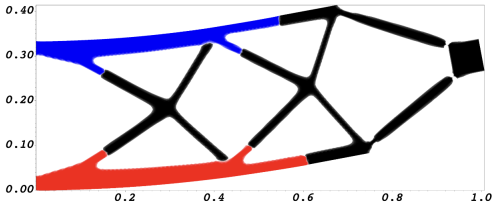

$t = 0.25$

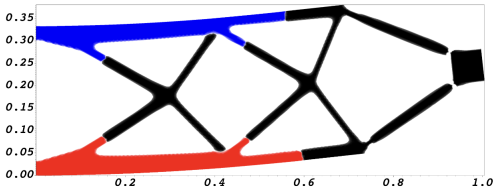

$t = 0.35$

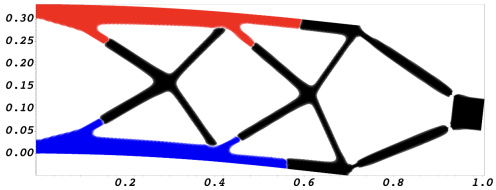

$t = 0.60$

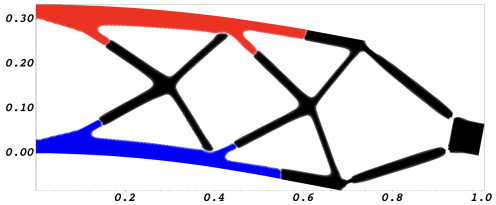

$t = 0.75$

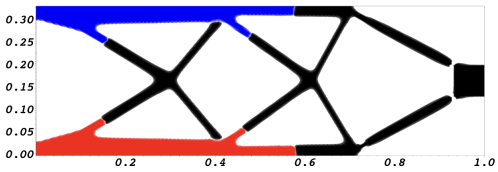

$t = 0.95$

Figure 5.10: Composite plot of both material density and the heat source in the deformed configuration (bottom) for stiffness ratio $E_3/E_2 = 1$. The red and blue represent the area of the responsive material with heat source values 1 and -1 respectively.

Chapter 6

Conclusion

To conclude, in this thesis we explored optimal design of responsive structures which exploit recent advances in materials and manufacturing. After a brief discussion on the ill-posedness of the optimal design problem, we considered a phase-field regularization as a means to gain well-posedness. After proving existences of solutions to our responsive design problem, we considered two concrete examples.

We started with the optimal design of compliant morphing structures where the stimulus is a design variable. We considered linear elastic materials whose constitutive laws depend on an external real-valued stimulus inducing an inelastic strain. Through this, we applied the well-known theorems of $\Gamma-$convergence to prove well-posedness of a class of carefully chosen objective functions. Then we applied direct methods of calculus of variations to find closed-form minimizers for our stimulus. We showed a variety of integrated responsive designs in 2D with varying ratios of stiffness between the responsive and non-responsive material while the stiffness for "void" is kept constant.

We then turned to optimal design of compliant morphing structures where the

stimulus itself is a state variable governed by a PDE. In this extension of our first example, we chose the poisson PDE and the transient heat PDE to control the stimulus. The later case gives rise to time-dependent responsive structures whose shape changes by the stimulus and time. This is the most computationally expensive problem as we first had to discretize the time into n time steps, and then in each iteration solve $4n$ PDEs before updating the design.

Bibliography

[1] R. Adams and J. Fournier. Sobolev spaces. *Elsevier*, 2003.

[2] A. Akerson, B. Bourdin, and K. Bhattacharya. Optimal design of responsive structures. *Structural and Multidisciplinary Optimization*, 65(4), mar 2022. doi: 10.1007/s00158-022-03200-5.

[3] G. Alberti. Variational models for phase transitions, an approach via Γ–convergence. In *Calculus of Variations and Partial Differential Equations*, pages 95–114, Berlin, 2000. Springer–Verlag. doi: 10.1007/978-3-642-57186-2_3.

[4] A. Alexanderian and I. Sunseri. Computing gradients and hessians using the adjoint method. *North Calorina State University*, 2019. URL `https://aalexan3.math.ncsu.edu/articles/adjoint_based_gradient_and_hessian.pdf`.

[5] G. Allaire. Shape optimization by the homogenization method. *Applied Mathematical Sciences*, 146(3):291–318, 2002.

[6] G. Allaire. Optimal design of structures map 562. *Lecture Notes*, 2015. URL `http://www.cmap.polytechnique.fr/~allaire/map562/`.

[7] G. Allaire and S. Aubry. On optimal microstructures for a plane shape optimization problem. *Structural optimization*, 17(2):86–94, 1999. doi: 10.1007/BF01195933.

[8] G. Allaire, E. Bonnetier, G. Francfort, , and F. Jouve. Shape optimization by the homogenization method. *Numerical Mathematics*, 76(1):27–68, 1997. doi: 10.1007/s002110050253.

[9] G. Allaire, F. Jouve, and H. Maillot. Topology optimization for minimum stress design with the homogenization method. *Structural and Multidisciplinary Optimization*, 28(2):87–98, 2004. doi: 10.1007/s00158-004-0442-8.

[10] G. Allaire, F. Jouve, and A.-M. Toader. Structural optimization using sensitivity analysis and a level-set method. *Journal of Computational Physics*, 194(1):363–393, 2004. doi: 10.1016/j.jcp.2003.09.032.

[11] G. Allaire, F. de Gournay, F. Jouve, and A.-M. Toader. Structural optimization using topological and shape sensitivity via a level set method. *Control and Cybernetics*, 34(1):59–80, 2005. URL `http://eudml.org/doc/209353`.

[12] G. Allaire, C. Dapogny, and P. Frey. A mesh evolution algorithm based on the level set method for geometry and topology optimization. *Structural and Multidisciplinary Optimization*, 48(4):711–715, apr 2013. doi: 10.1007/s00158-013-0929-2.

[13] M. S. Alnæs. *UFL: a finite element form language*, pages 303–338. Springer Berlin Heidelberg, Berlin, Heidelberg, 2012. ISBN 978-3-642-23099-8. doi: 10.1007/978-3-642-23099-8_17.

[14] M. S. Alnæs, A. Logg, K. B. Ølgaard, M. E. Rognes, and G. N. Wells. Unified form language: A domain-specific language for weak formulations of partial differential equations. *ACM Transactions on Mathematical Software*, 40(2), mar 2014. ISSN 0098-3500. doi: 10.1145/2566630.

[15] L. Ambrosio. Existence theory for a new class of variational problems. *Archive for Rational Mechanics and Analysis*, 111(4):291–322, 1990. doi: 10.1007/BF00376024.

[16] L. Ambrosio and G. Buttazzo. An optimal design problem with perimeter penalization. *Calculation of Variations. Partial Differential Equations*, 1(1):55–59, 1993. doi: 10.1007/BF02163264.

[17] L. Ambrosio, N. Fusco, and D. Pallara. *Functions of Bounded Variation and Free Discontinuity Problems*. Oxford University Press, New York, 2000. doi: 10.1093/oso/9780198502456.001.0001.

[18] S. Balay, W. D. Gropp, L. C. McInnes, and B. F. Smith. Efficient management of parallelism in object oriented numerical software libraries. In E. Arge, A. M. Bruaset, and H. P. Langtangen, editors, *Modern Software Tools in Scientific Computing*, pages 163–202. Birkhäuser Press, 1997.

[19] S. Balay, S. Abhyankar, M. F. Adams, S. Benson, J. Brown, P. Brune, K. Buschelman, E. Constantinescu, L. Dalcin, A. Dener, V. Eijkhout, J. Faibussowitsch, W. D. Gropp, V. Hapla, T. Isaac, P. Jolivet, D. Karpeev, D. Kaushik, M. G. Knepley, F. Kong, S. Kruger, D. A. May, L. C. McInnes, R. T. Mills, L. Mitchell, T. Munson, J. E. Roman, K. Rupp, P. Sanan, J. Sarich, B. F. Smith, S. Zampini,

H. Zhang, H. Zhang, and J. Zhang. PETSc/TAO users manual. Technical Report ANL-21/39 - Revision 3.21, Argonne National Laboratory, 2024.

[20] S. Balay, S. Abhyankar, M. F. Adams, S. Benson, J. Brown, P. Brune, K. Buschelman, E. M. Constantinescu, L. Dalcin, A. Dener, V. Eijkhout, J. Faibussowitsch, W. D. Gropp, V. Hapla, T. Isaac, P. Jolivet, D. Karpeev, D. Kaushik, M. G. Knepley, F. Kong, S. Kruger, D. A. May, L. C. McInnes, R. T. Mills, L. Mitchell, T. Munson, J. E. Roman, K. Rupp, P. Sanan, J. Sarich, B. F. Smith, S. Zampini, H. Zhang, H. Zhang, and J. Zhang. PETSc Web page. `https://petsc.org/`, 2024. URL `https://petsc.org/`.

[21] M. Bendsøe and O. Sigmund. Material interpolation schemes in topology optimization. *Archive of Applied Mechanics*, 69:635–654, 1999. doi: 10.1007/s004190050248.

[22] M. Bendsøe, A. Díaz, and N. Kikuchi. *Topology and Generalized Layout Optimization of Elastic Structures*, pages 159–205. Springer Netherlands, Dordrecht, 1993. doi: 10.1007/978-94-011-1804-0_13.

[23] M. Bendsøe. Optimal shape design as a material distribution problem. *Structural optimization*, 1(4):193–202, 1989. doi: 10.1007/BF01650949.

[24] M. Bendsøe and P. Duysinx. Topology optimization of continuum structures with stress constraints. *International Journal for Numerical Methods in Engineering*, 34:1453–1478, 1998.

[25] M. Bendsøe and O. Sigmund. Topology optimization: Theory, methods and applications. *Springer, New York*, 2nd edition, 2003.

[26] E. Birgin and J. Martinez. *Practical Augmented Lagrangian Methods for Constrained Optimization*. Society for Industrial and Applied Mathematics, 2014.

[27] B. Bourdin. Filters in topology optimization. *International Journal for Numerical Methods in Engineering*, 50:2143–2158, 2001. doi: 10.1002/nme.116.

[28] B. Bourdin and A. Chambolle. Design-dependent loads in topology optimization. *ESAIM: Control, Optimisation and Calculus of Variations*, 9:19–48, 2003. doi: 10.1051/cocv:2002070.

[29] B. Bourdin and A. Chambolle. The phase-field method in optimal design. *Solid Mechanics and its Applications*, pages 207–215, 2006. doi: 10.1007/1-4020-4752-5_21.

[30] S. Boyd and L. Vandenberghe. *Convex optimization*. Cambridge University Press, 2004.

[31] A. Braides. Approximation of free-discontinuity problems. *Springer. Lecture Notes in Mathematics*, 1694, 1998.

[32] A. Braides. $\Gamma-$convergence for beginners. *Oxford University Pres*, 22, 2002.

[33] S. Brenner and L. Scott. *The mathematical theory of finite element methods*, volume 15. Springer Verlag, 2008.

[34] H. Brezis. *Functional Analysis, Sobolev Spaces and Partial Differential Equations*. Springer, 2010.

[35] A. Cherkaev. Variational methods for structural optimization. *Applied Mathematical Sciences*, Volume 140, 2000.

[36] P. G. Ciarlet. *The Finite Element Method for Elliptic Problems.* Society for Industrial and Applied Mathematics, 2002.

[37] P. G. Ciarlet. *Linear and Nonlinear Functional Analysis with Applications.* SIAM, Philadelphia, 2013. doi: 10.1137/1.9781611972597.fm.

[38] B. Dacorogna. *Direct Methods in the Calculus of Variations.* Applied Mathematical Sciences. Springer Berlin Heidelberg., 1989.

[39] G. Dal Maso. An introduction to $\Gamma-$convergence. *Springer*, 2023.

[40] E. De Giorgi. Sulla convergenza di alcune successioni di integrali del tipo dell'are. *Rendiconti del Circolo Matematico di Palermo*, 8:277–294, 1975.

[41] E. De Giorgi and T. Franzoni. Su un tipo di convergenza variazional. *Atti della Accademia Nazionale dei Lincei. Rendiconti Lincei. Matematica e Applicazioni*, 58:842–850, 1975.

[42] E. De Giorgi and S. Spagnolo. Sulla convergenza degli integrali dell'energia per operatori ellittici del secondo ordine. *Bollettino dell'Unione Matematica Italiana*, 8:391–411, 1973.

[43] J. C. De Los Reyes. Numerical pde-constrained optimization. *SpringerBriefs in Optimization*, Springer, 2015.

[44] D. Dyck and D. Lowther. Automated design of magnetic devices by optimizing material distribution. *IEEE Transactions on Magnetics*, 32(3):1188–1193, 1996. doi: 10.1109/20.497456.

[45] H. A. Eschenauer and N. Olhoff. Topology optimization of continuum structures: A review. *Applied Mechanics Review*, 54(4), 2022. doi: 10.1115/1.1388075.

[46] L. C. Evans. *Partial differential equations*. American Mathematical Society, Providence, R.I., 2010. ISBN 9780821849743 0821849743.

[47] G. A. Francfort and F. Murat. Homogenization and optimal bounds in linear elasticity. *Archive for Rational Mechanics and Analysis*, 94(4):307–334, 1986. doi: 10.1007/BF00280908.

[48] O. Ghattas. Lecture notes: Computational and variational inverse problems. *University of Texas at Austin*, 2015. URL `https://users.oden.utexas.edu/~omar/inverse_problems/Sensitivity_Analysis_Notes.pdf`.

[49] L. Giovanni. A first course in sobolev spaces. *American Mathematical Society*, 2nd edition, 2017.

[50] R. Haber, C. Jog, and M. Bendsøe. A new approach to variable-topology shape design using a constraint on the perimeter. *Structural and Multidisciplinary Optimization*, 11:1–12, 1996. doi: 10.1007/BF01279647.

[51] D. A. Ham, P. H. J. Kelly, L. Mitchell, C. J. Cotter, R. C. Kirby, K. Sagiyama, N. Bouziani, S. Vorderwuelbecke, T. J. Gregory, J. Betteridge, D. R. Shapero, R. W. Nixon-Hill, C. J. Ward, P. E. Farrell, P. D. Brubeck, I. Marsden, T. H. Gibson, M. Homolya, T. Sun, A. T. T. McRae, F. Luporini, A. Gregory, M. Lange, S. W. Funke, F. Rathgeber, G.-T. Bercea, and G. R. Markall. Firedrake user manual. *Imperial College London and University of Oxford and Baylor University and University of Washington*, 5 2023. doi: 10.25561/104839.

[52] J. Jonsmann, O. Sigmund, and S. Bouwstra. Compliant thermal microactuators. *Sensors and Actuators*, 7:463–469, 1999. doi: 10.1016/S0924-4247(99)00011-4.

[53] D. Kinderlehrer and G. Stampacchia. *An introduction to variational inequalities and their applications, classics in applied mathematics,*, volume 31. SIAM, Philadelphia, PA, 1989.

[54] R. Kohn and G. Strang. Optimal design and relaxation of variational problems. *Communications on Pure and Applied Mathematics*, 39(1):113–137, 1986. doi: 10.1002/cpa.3160390107.

[55] A. J. Kurdila and M. Zabarankin. *Convex Functional Analysis*. Springer, 2005.

[56] U. Larsen, O. Sigmund, and S. Bouwstra. Design and fabrication of micromechanisms and structures with negative Poisson's ratio. *Journal of Microelectromechanical Systems*, 6(2):99–106, 1997. doi: 10.1109/84.585787.

[57] R. Lipton and M. Stuebner. Optimization of composite structures subject to local stress constraints. *Computer Methods in Applied Mechanics and Engineering*, 196 (1-3):66–75, 2006. doi: 10.1016/j.cma.2006.01.012.

[58] A. Logg, K.-A. Mardal, G. N. Wells, et al. *Automated Solution of Differential Equations by the Finite Element Method*. Springer, 2012. doi: 10.1007/978-3-642-23099-8.

[59] J. Logo and H. Ismail. Milestones in the 150-year history of topology optimization: A review. *Computer Assisted Methods in Engineering and Science*, 27(2–3): 97–132, 2020. ISSN 2956-5839. doi: 10.24423/cames.296.

[60] J. C. Maxwell. I.—on reciprocal figures, frames, and diagrams of forces. *Transactions of the Royal Society of Edinburgh*, 26(1):1–40, 1870. doi: 10.1017/S0080456800026351.

[61] L. Modica. The gradient theory of phase transitions and the minimal interface criterion. *The Archive for Rational Mechanics and Analysis*, 98(2):123–142, 1987. doi: 10.1007/BF00251230.

[62] L. Modica and S. Mortola. Un esempio di $\Gamma-$convergenza. *Bollettino dell'Unione Matematica Italiana*, 14(1):285–299, 1977.

[63] L. Modica and S. Mortola. Il limite nella Γ–convergenza di una famiglia di funzionali ellittici. *Bollettino dell'Unione Matematica Italiana*, 14(3):526–529, 1977.

[64] J. J. Moré and D. J. Thuente. Line search algorithms with guaranteed sufficient decrease. *ACM Transactions on Mathematical Software*, 20(3):286–307, 1994. doi: 10.1145/192115.192132.

[65] P. Penzler, M. Rumpf, and B. Wirth. A phase-field model for compliance shape optimization in nonlinear elasticity. *ESAIM: Control, Optimisation and Calculus of Variations*, 18(1):229–258, 2012. doi: 10.1051/cocv/2010045.

[66] J. Petersson. Some convergence results in perimeter-controlled topology optimization. *Computer Methods in Applied Mechanics and Engineering*, 171:123–140, 1999. doi: 10.1016/S0045-7825(98)00248-5.

[67] R. Plessix. A review of the adjoint-state method for computing the gradient of

a functional with geophysical applications. *Geophysical Journal International*, 167:495–503, 2006. doi: 10.1111/j.1365-246X.2006.02978.x.

[68] F. Rindler. Calculus of variations. *Springer*, 2018.

[69] H. Rodrigue, W. Wang, B. Bhandari, and S.-H. Ahn. Fabrication of wrist-like sma-based actuator by double smart soft composite casting. *Smart Materials and Structures*, 24:125003, 2015. doi: 10.1088/0964-1726/24/12/125003.

[70] F. Santambrogio. A course in the calculus of variations: Optimization, regularity, and modeling. *Springer*, 2023.

[71] T. A. Schaedler, A. J. Jacobsen, A. Torrents, A. E. Sorensen, J. Lian, J. R. Greer, L. Valdevit, and W. B. Carter. Ultralight metallic microlattices. *Science*, 334(6058):962–965, 2011. doi: 10.1126/science.1211649.

[72] J. Shabani, K. Bhattacharya, and B. Bourdin. Systematic design of compliant morphing structures: a phase-field approach. *Applied Mathematics and Optimization*, 2024 (Submitted for publication).

[73] O. Sigmund. On the design of compliant mechanisms using topology optimization. *Mechanics of Structures and Machines*, 25(4):495–526, 1997. doi: 10.1080/08905459708945415.

[74] O. Sigmund. Design of multiphysics actuators using topology optimization – part i: One-material structures. *Computer Methods in Applied Mechanics and Engineering*, 190(49):6577–6604, 2001. doi: 10.1016/S0045-7825(01)00251-1.

[75] O. Sigmund. Design of multiphysics actuators using topology optimization –

part ii: Two-material structures. *Computer Methods in Applied Mechanics and Engineering*, 190(49):6605–6627, 2001. doi: 10.1016/S0045-7825(01)00252-3.

[76] O. Sigmund and K. Maute. Topology optimization approaches. *Structural and Multidisciplinary Optimization*, 48(6):1031–1055, 2013. doi: 10.1007/s00158-013-0978-6.

[77] B. Sisto. Minimal interface criterion for phase transitions in mixtures of cahn-hilliard fluids. *Annales de l'Institut Henri Poincaré C, Analyse non linéaire*, 7 (2):67–90, 1990. doi: 10.1016/S0294-1449(16)30304-3.

[78] P. Sternberg. The effect of a singular perturbation on nonconvex variational problems. *Archive for Rational Mechanics and Analysis*, 101(3):209–260, 1988. doi: 10.1007/BF00253122.

[79] K. Suzuki and N. Kikuchi. A homogenization method for shape and topology optimization. *Computer Methods in Applied Mechanics and Engineering*, 93(3): 291–318, 1991. doi: 10.1016/0045-7825(91)90245-2.

[80] S. Ta'asan. Introduction to shape design and control. *Carnegie Mellon University*, 1997. URL `https://www.math.cmu.edu/~shlomo/VKI-Lectures/lecture1/index.html`.

[81] A. Takezawa, S. Nishiwaki, and M. Kitamura. Shape and topology optimization based on the phase field method and sensitivity analysis. *Journal of Computational Physics*, 229(7):2697–2718, 2010. doi: 10.1016/j.jcp.2009.12.017.

[82] N. V. Tran and B. Bourdin. Minimum compliance with obstacle constraints: an

active set approach. *Structural and Multidisciplinary Optimization*, 65(4), 2022. doi: 10.1007/s00158-022-03199-9.

[83] M. Y. Wang and S. Zhou. Synthesis of shape and topology of multi-material structures with a phase-field method. *Journal of Computer-Aided Materials Design*, 11(2-3):117–138, 2004. doi: 10.1007/s10820-005-3169-y.

[84] M. Y. Wang and S. Zhou. Phase field: A variational method for structural topology optimization. *Computer Modeling in Engineering & Sciences*, 6(6): 547–566, 2004. doi: 10.3970/cmes.2004.006.547.

[85] T. Xu, J. Zhang, M. Salehizadeh, O. Onaizah, and E. Diller. Millimeter-scale flexible robots with programmable three-dimensional magnetization and motions. *Science Robotics*, 4(29), 2019. doi: 10.1126/scirobotics.aav4494.

[86] S. W. Zhou and M. Y. Wang. Multimaterial structural topology optimization with a generalized Cahn-Hilliard model of multiphase transition. *Structural Multidisciplinary Optimization*, 33(2):89–111, 2007. doi: 10.1007/s00158-006-0035-9.